AD-A127 253 ACOUSTIC NDE OF MULTILAYERED COMPOSITES PHASE II ANGLE 1/1
BEAM MODEL VALIDAT..(U) TETRA TECH INC ARLINGTON VA
R SHANKAR ET AL. MAR 83 TETRAT-TC-6139 N60921-81-C-0300
UNCLASSIFIED F/G 14/2 NL

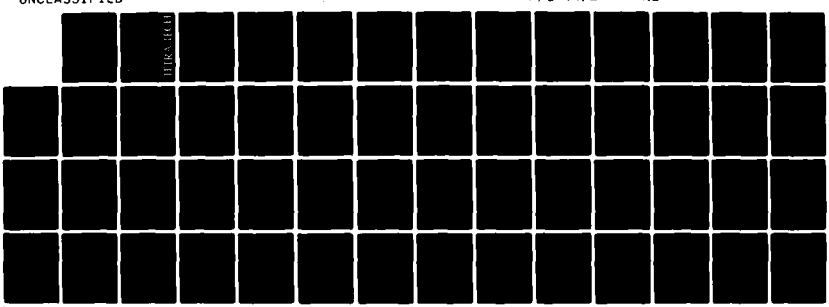

END
DATE FILMED
5-83
DTIC

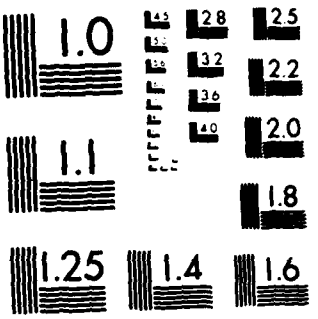

(12)

TETRA TECH

ACOUSTIC NDE OF MULTILAYERED COMPOSITES

PHASE 2
ANGLE BEAM MODEL VALIDATION AND INSPECTION OF BRONZE-RUBBER STRUCTURES

FINAL TECHNICAL REPORT

March 1983

TC-6139

ACOUSTIC NDE OF MULTILAYERED COMPOSITES

PHASE 2: ANGLE BEAM MODEL VALIDATION AND INSPECTION OF BRONZE-RUBBER STRUCTURES

FINAL TECHNICAL REPORT

Prepared Under Contract N-60921-81-C-0300

Period Covered: July 1982 - January 1983

Prepared by:

Ramesh Shankar, Ph.D.
Stephen S. Lane, Ph.D.

Tetra Tech, Inc.
1911 N. Ft. Myer Drive
Arlington, Virginia 22209

REPORT DOCUMENTATION PAGE

UNCLASSIFIED

READ INSTRUCTIONS BEFORE COMPLETING FORM

1. REPORT NUMBER	2. GOVT ACCESSION NO.	3. RECIPIENT'S CATALOG NUMBER
	AD-A127 253	

4. TITLE (and Subtitle)
Acoustic NDE of Multilayered Composites
Phase II: Angle Beam Model Validation and Inspection of Bronze-Rubber Structures

5. TYPE OF REPORT & PERIOD COVERED
Final Report for Period
July 1982 - January 1983

6. PERFORMING ORG. REPORT NUMBER
TC-6139

7. AUTHOR(s)
Ramesh Shankar
Stephen S. Lane

8. CONTRACT OR GRANT NUMBER(s)
N-60921-81-C-0300

9. PERFORMING ORGANIZATION NAME AND ADDRESS
Tetra Tech, Inc.
1911 N. Ft. Myer Drive, Suite 601
Arlington, VA 22209

10. PROGRAM ELEMENT, PROJECT, TASK AREA & WORK UNIT NUMBERS

11. CONTROLLING OFFICE NAME AND ADDRESS
Naval Surface Weapons Center
White Oak, MD 20910
Code: R34, Materials Evaluation

12. REPORT DATE
March 1983

13. NUMBER OF PAGES
42

14. MONITORING AGENCY NAME & ADDRESS *(if different from Controlling Office)*

15. SECURITY CLASS. *(of this report)*
UNCLASSIFIED

15a. DECLASSIFICATION/DOWNGRADING SCHEDULE

16. DISTRIBUTION STATEMENT *(of this Report)*
Approved for Public Release; Distribution Unlimited.

17. DISTRIBUTION STATEMENT *(of the abstract entered in Block 20, if different from Report)*

18. SUPPLEMENTARY NOTES

19. KEY WORDS *(Continue on reverse side if necessary and identify by block number)*
Nondestructive Evaluation, Multilayered Structures, Acoustic Modeling, Lattice Filter, Angled Beam Inspection, Attenuation, Mode Conversion, Digital Data Acquisition, Signal Processing, Filtering, Deconvolution, Cepstral Filtering

20. ABSTRACT *(Continue on reverse side if necessary and identify by block number)*
A model for the reponse of layered structures to off-normal ultrasonic pulses was validated by modifying the computer model developed under Phase 1 of this contract. For angle beams, the repsonses have different magnitude and phases, and include different modes of propagation, unlike the case for normal-incidence beams investigated under Phase 1. The model-simulated reflection series was compared with ultrasonic digital data collected from a bronze-epoxy-aluminum structure. The response from the different interfaces and for different transit paths were validated for their (i) transit time, (ii) mode of propagation and (iii) relative

DD FORM 1 JAN 73 1473 EDITION OF 1 NOV 65 IS OBSOLETE
S/N 0102-014-6601

UNCLASSIFIED
SECURITY CLASSIFICATION OF THIS PAGE (When Data Entered)

cont

magnitude and phase.

The angle beam model was used to design a procedure to inspect bronze-epoxy-rubber multilayered structures. The design yielded an inspection mode with shear waves in bronze and longitudinal waves in rubber, and a shear wave angle of 32° in bronze, using 1MHz, pitch-catch transducers. At this angle, the longitudinal wave in bronze was beyond critical and, while both shear and longitudinal waves propagated in rubber, the former were attenuated enough to not affect the results. At this angle, the model predicted maximum signals for "flaw" and "no-flaw" conditions at the bottom of rubber, i.e., lack of adherent and good adherent, which optimizes detection. A maximum phase difference for these two conditions was also maintained, for optimum discrimination.

Ultrasonic digital data were collected under flaw and no-flaw conditions. The data were processed and the flaw and no-flaw signals were clearly separable.

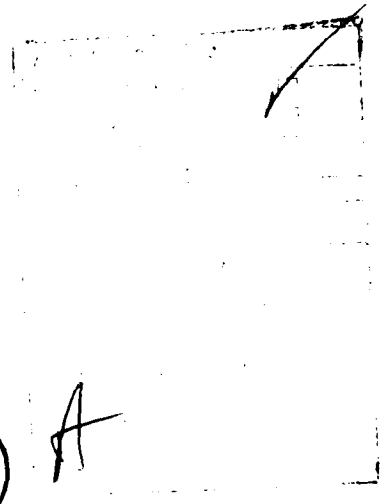

FOREWORD

This final report covers work performed during the period July 1982 through January 1983 under contract N-60921-C-0300, "Acoustic NDE of Multilayered Composites."

Mr. Cliff Anderson, R34, was the program monitor. The authors thank Mr. Anderson for his guidance. Mr. Jeffrey M. Warren and Ms. Susan N. Vernon, R34, were instrumental in assisting the authors in data collection and digitization. Their contributions are gratefully acknowledged.

Dr. Ramesh Shankar was the program manager and principal investigator.

ABSTRACT

A model for the response of layered structures to off-normal ultrasonic pulses was validated by modifying the computer model developed under Phase 1 of this contract. For angle beams, the responses have different magnitude and phases, and include different modes of propagation, unlike the case for normal-incidence beams investigated under Phase 1. The model-simulated reflection series was compared with ultrasonic digital data collected from a bronze-epoxy-aluminum structure. The response from the different interfaces and for different transit paths were validated for their (i) transit time, (ii) mode of propagation and (iii) relative magnitude and phase.

The angle beam model was used to design a procedure to inspect bronze-epoxy-rubber multilayered structures. The design yielded an inspection mode with shear waves in bronze and longitudinal waves in rubber, and a shear wave angle of 32° in bronze, using 1MHz, pitch-catch transducers. At this angle, the longitudinal wave in bronze was beyond critical and, while both shear and longitudinal waves propagated in rubber, the former were attenuated enough to not affect the results. At this angle, the model predicted maximum signals for "flaw" and "no-flaw" conditions at the bottom of rubber, i.e., lack of adherent and good adherent, which optimizes detection. A maximum phase difference for these two conditions was also maintained, for optimum discrimination.

Ultrasonic digital data were collected under flaw and no-flaw conditions. The data were processed and the flaw and no-flaw signals were clearly separable.

TABLE OF CONTENTS

LIST OF FIGURES

SUMMARY OF RESULTS

A computer model was developed to predict the magnitude and phase of the acoustic responses from different interfaces of an arbitrary multilayered structure. As inputs to the model, the individual layer's acoustic parameters, and mode of propagation are specified as well as the incident beam angle to the top layer. The model generates a complex reflection series as its output, where the independent axis is either time or travel path and the ordinate is the magnitude of the response.

The model was validated with ultrasonic digital data collected from a sample bronze-expoxy-aluminum specimen. Figure 1 shows in phasor form, the experimentally observed and model predicted magnitude and phases of six responses for a 33° shear wave in bronze. The nomenclature of the responses are of the form (1,m,n), where l is the number of round trip paths in bronze and m and n the number of paths, respectively, in epoxy and aluminum. A (1,1,1) path, for example, has transited each of the layers 1 time, with a 33° beam angle shear wave in bronze, a 37° longitudinal wave in epoxy, and 44° shear wave in aluminum.

There is close correspondence between experimental measurements and model predicted values.

The model was then used for designing procedures for inspecting bronze-epoxy-rubber multilayer parts for flaws in the bottom rubber layer (lack of adhesion). The design procedure yielded an optimum angle of 33° shear wave in bronze (longitudinal wave was beyond critical), and from Snell's law, a 38° longitudinal wave in epoxy, and a 36° longitudinal wave in rubber.

Figure 2 shows the signals received from this specimen under no flaw and flaw conditions at the bottom of rubber. Figure 3 shows the no flaw signal compared to the difference signal under no flaw and flaw conditions. A large response due to a flaw can be discerned at about 5 and 7 μs.

It is concluded that the model was successfully validated and the results used to design an optimum procedure for inspecting bronze-epoxy-rubber parts.

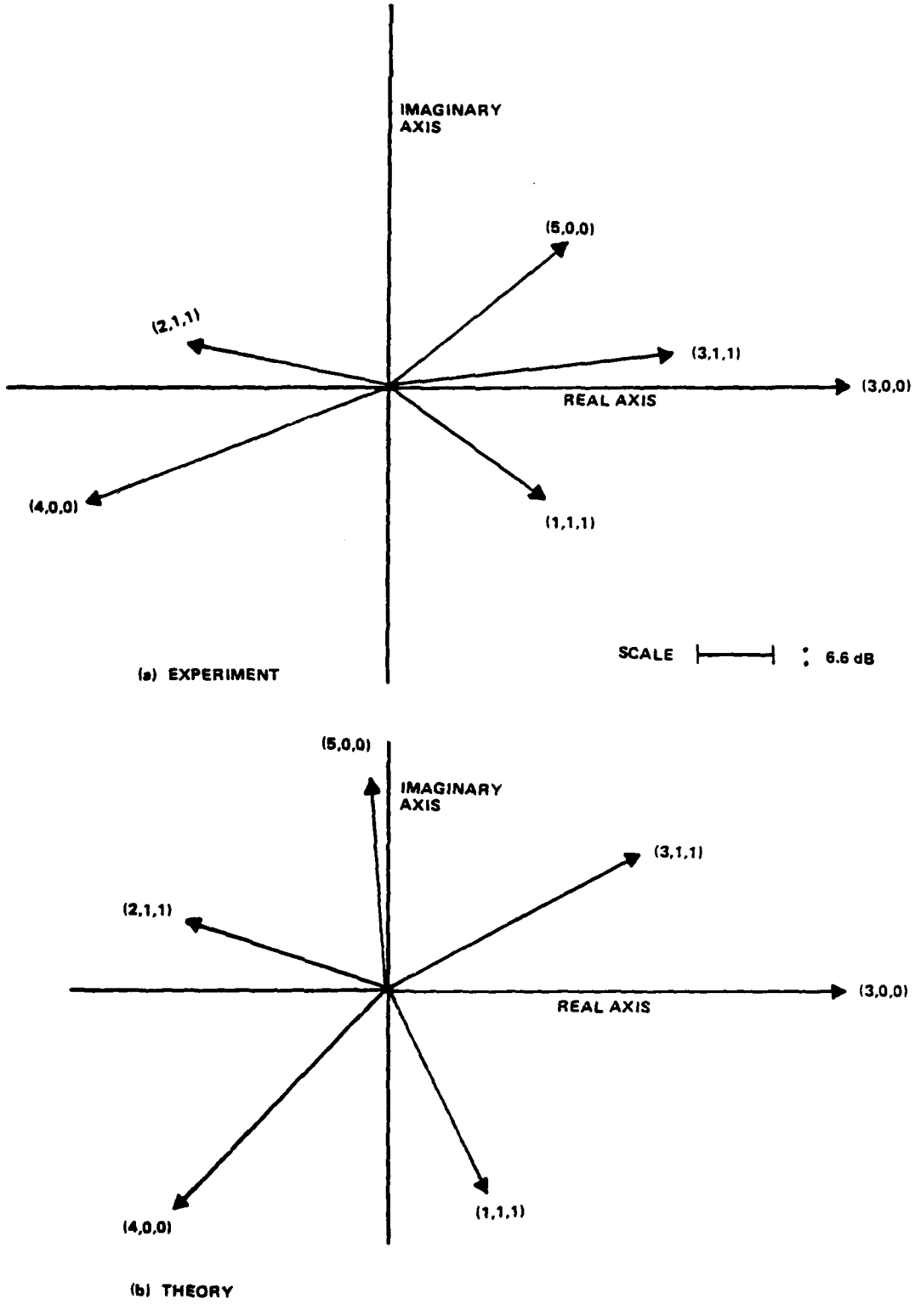

Figure 1. PHASOR COMPARISON BETWEEN EXPERIMENT AND THEORY FOR SIX RESPONSES FROM A BRONZE-EPOXY-ALUMINUM STRUCTURES

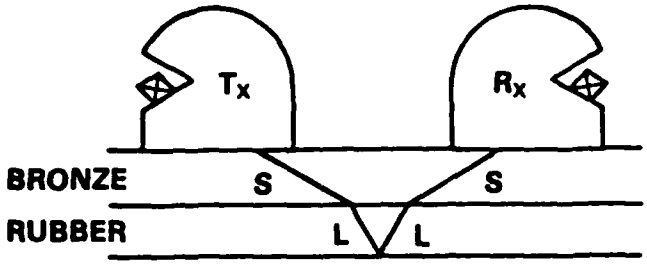

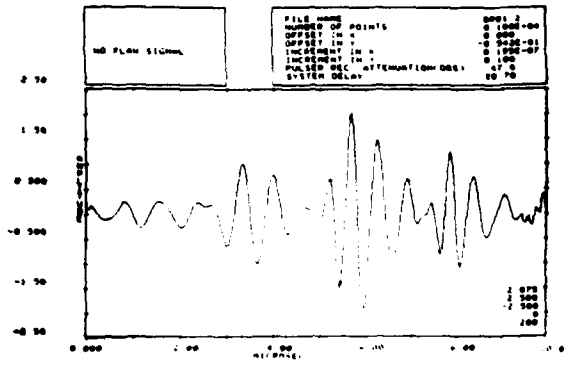

NO FLAW

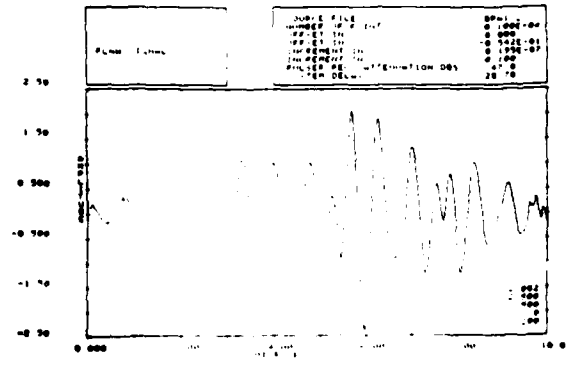

FLAW

T_X AND R_X FREQUENCIES: 1 MHZ
BEAM ANGLE IN BRONZE ≈ 32°
BEAM ANGLE IN RUBBER ≈ 28°

Figure 2. INSPECTION OF TWO LAYERS FOR FLAW AT BOTTOM OF RUBBER

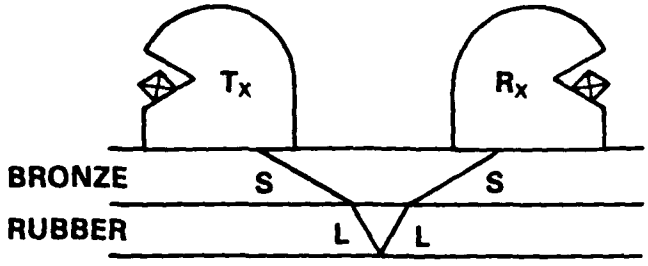

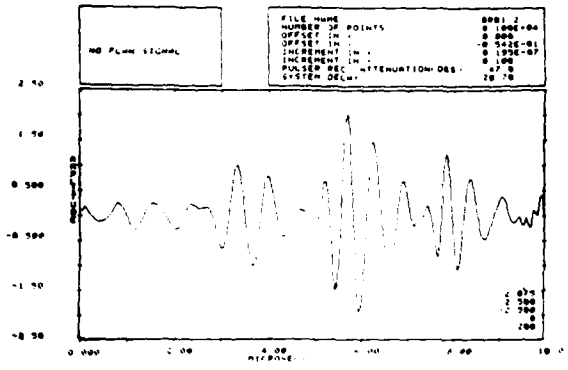

NO FLAW

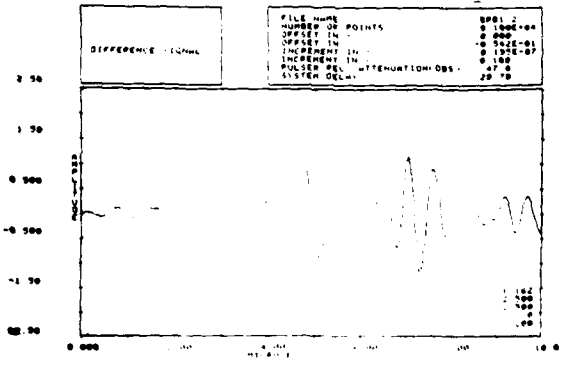

DIFFERENCE

T_X AND R_X FREQUENCIES: 1 MHZ
BEAM ANGLE IN BRONZE ≈ 32°
BEAM ANGLE IN RUBBER ≈ 28°.

Figure 3. NO–FLAW AND DIFFERENCE SIGNALS (FLAW RESPONSE IN DIFFERENCE SIGNAL AT 5 AND 7 μs

ANGLE BEAM MULTILAYERED MODEL

1.1 BACKGROUND AND OVERVIEW

Conventional ultrasonic NDE of multilayered components for bond integrity is performed by employing normal-incidence pulse echo methods. Some components are designed so that the acoustic transit times in the intervening layers are almost identical, causing the signals from different layers to overlap, and making signal interpretation very difficult. To decouple the arrival times, angle beam inspection methods are used with a pair of transducers located spatially apart, and with off-normal beam incident angles. However, signal interpretation may still be difficult because of mixed mode propagation within each layer (i.e., shear and longitudinal) at angles off-normal and because of to mode conversion at each interface.

In order to develop a consistent and methodological approach to multilayered NDE, the U.S. Navy initiated the second phase of a project with Tetra Tech to develop and validate a generic computer-based model for angle beam inspection. In the first phase Tetra Tech developed a computer-based normal-incident multilayer model using techniques developed in geophysics [1]. In [1] it was also shown that the model, written in FORTRAN IV for a general purpose computer, was applicable for off-normal incident excitation, with receiver in pulse-echo or pitch-catch mode. In addition, the model considered the effects of attenuation in each layer and of mode conversion, for off-normal beams, on the received signal.

This report documents further work performed in validating the model with ultrasonic data collected and digitized from bronze-aluminum multilayer parts; the specimen was selected because of the relative lack of signal attenuation in each material. In addition, the model output was used successfully to design a data collection procedure to inspect bronze-rubber multilayered parts for flaws at the bottom of the first rubber layer. The design included the optimum beam angles and transducer frequency to maximize the response under flaw and no-flaw conditions at the bottom of the first rubber layer. Data processing results are shown wherein discrimination between "good" bond and lack of adherent was successfully performed.

A pair of transducers was selected and a lucite wedge fabricated according to specifications. Ultrasonic data were collected and digitized from bronze-rubber multilayered specimens. The signals were processed in an attempt to distinguish flaws.

The report documents the methods used for model validation and the results in inspecting bronze-rubber multilayered specimens.

1.2 WAVE PROPAGATION AT OFF-NORMAL INCIDENCE

The development presented in Reference 1, Equation 3.5 and 3.6 leads to the general matrix equation for arbitrary reflection and transmission coeffecients:

$$\begin{bmatrix} D_k(z) \\ U_k(z) \end{bmatrix} = \frac{z^{N_k}}{T_k'} \begin{bmatrix} z^{-2N_k} & z^{-2N_k} \\ -R_k & R_k z^{-2N_k} \end{bmatrix} \begin{bmatrix} D_{k+1}(z) \\ U_{k+1}(z) \end{bmatrix} \qquad 1.0$$

The symbols D and U represent the amplitudes of the downgoing and upgoing waves, respectively. The subscripts k and k+1 refer to, respectively, the kth and (k+1)st layer. The term N_k represents the number of sampled units of delay which is a function of sampling interval, acoustic velocity, and layer thickness. The arguments z of D and U refers to the sampled z-domain representation which was shown in Reference 1 to be convenient for computer implementation. So, a delay term is manifest as an exponent of z, i.e., z^{-2N_k}, refers to a delay of $2N_k$ units. The four coefficients R_k, R_k', T_k and T_k' are:

R_k: acoustic impedance for a downgoing wave from k to (k+1)

R_k': impedance for an upgoing wave from (k+1) to k

T_k: transmission coefficient for a downgoing wave from k to (k+1)

T_k': transmission coefficient for an upgoing wave from (k+1) to k.

For the normal incidence case

$$R_k = -R_k', \quad T_k = 1 - R_k$$

and

$$T_k T_k' - R_k R_k' = 1$$

and the matrix equation reduces to Equation 3.11 in Reference 1.

However, the equation can be modified to account for the case where the ultrasonic energy is incident at any angle from the normal. For such off-normal incidence several new effects occur, among them the presence of mode converted energy in solids. That is, at angles other than zero, energy is converted from shear to compressional waves and vice versa, when a wave strikes a boundary.

The analysis presented here will not be complete, in that not all modes will be accounted for. However, it will be seen that the neglected modes are unimportant in this application.

The development of the matrix formulation of the arrival times and amplitudes presented in [1] did not depend explicitly on normal incidence. All that was assumed was a reflection and transmission coefficient at each boundary, and a time delay within each layer. These quantities take on particularly simple forms for the normal incidence case, but they can be calculated for the off-normal incidence case and can be included in the model as before.

To illustrate this point, refer to Figure 1.1. A wave propagates downward through medium 1, and is reflected and transmitted at an interface. Wave paths are drawn in their correct relation to boundaries. For the moment mode conversion is ignored. For off-normal incidence, the travel path in each layer is found by dividing the path length for normal incidence by the cosine

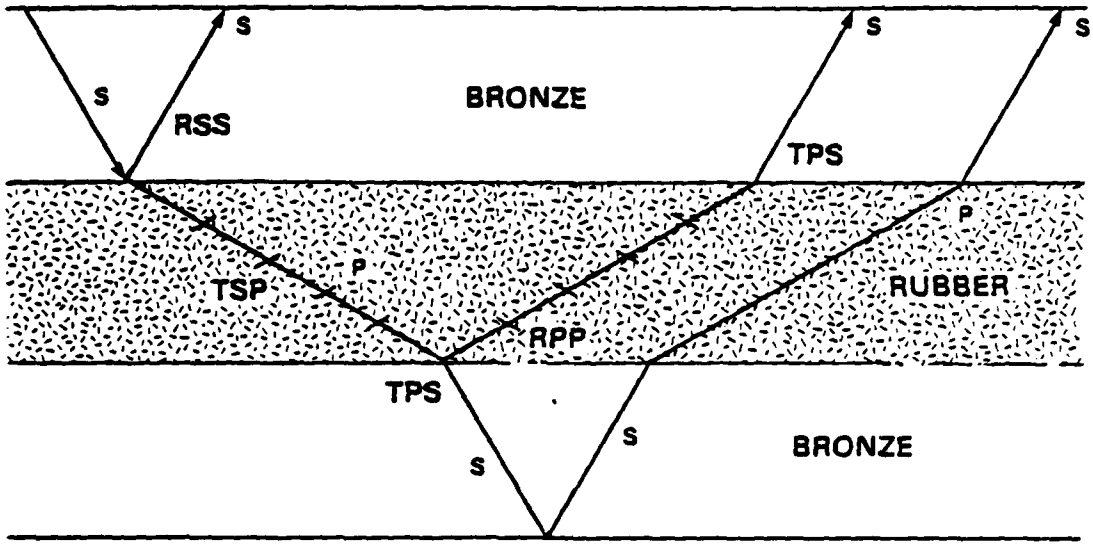

Figure 1.1 ANGLE BEAM INSPECTION

of the angle with respect to the normal of the sound beam in that layer as shown in Figure 1.1.

The reflection and transmission coefficients, Equations 3.1 and 3.2, Reference 1, are also modified for the off-normal incidence case. Three important effects are present for the case where two solids abut one another. First, at most angles a wave incident on the boundary in one medium will give rise to two waves in that medium, and two waves in the medium on the far side of the boundary. These waves are required for solid-solid boundaries to satisfy the conditions of continuity of displacement and stress everywhere.

Second, over certain angular ranges, some of the reflected waves do not propagate into either medium, but are confined to the boundary between media. They are never detected by a transducer on the surface, but carry energy away from the interface, and must be considered in order to correctly predict the amplitudes at the surface.

Finally, over the range where the waves referred to above are confined to the boundary, the reflection and transmission coefficients are complex. This means that each frequency component of the incident wave suffers a time delay upon reflection or transmission, and this delay is frequency dependent. The emerging pulse (if a pulse is incident, as is usually the case) is dispersed, and this must be accounted for when amplitudes are calculated.

The above simple theory, which accounts for only one wave in each medium, may be used when in fact two waves are actually present in each. First some notations are introduced. Reflection coefficients for compressional waves not converted to shear waves, but remain compressional waves, are denoted as R_{pp}. Here the conventional *seismic notation* p for compressional waves and s for shear waves is used. Where mode conversion to shear waves takes place, the reflection coefficient is denoted by R_{ps}. Similarly, reflection without mode conversion for an incident shear wave is associated with a reflection coefficient R_{ss} and that with mode conversion to p waves with R_{sp}. Transmission coefficients T are assigned the same notation. Thus T_{sp} refers to the amplitude of a wave which undergoes conversion from an s wave to a p wave as it crosses a boundary, and so on.

If all eight coefficients at each boundary (four for downgoing waves and four for upgoing waves) are calculated correctly, and the wave to be tracked in each layer is picked (the theory can handle only one per layer) the proper coefficients to use in Equation 1.0 can be selected to predict the amplitudes of these waves. For example, suppose the interest is in shear waves in layer 1 and compressional waves in layer 2. Then R_{ss} and T_{sp} for waves travelling downward from layer 1 to layer 2 are needed. Waves corresponding to R_{sp}, and to T_{ss} exist, but will be ignored. The coefficient R_{pp} and T_{ps} for waves traveling upward in the second layer are also needed. Again the waves related to two other coefficients are ignored. With these coefficients, and the modified time delays in each layer, Equation 1.0 can be used to predict amplitudes and times of arrival in this two-layered structure which consists of shear waves in the first layer and compressional waves in the second.

This example is not so unrealistic as it might seem at first. If the angle in the first layer, which is bronze, is selected beyond the critical

angle, there will be no compressional wave in the bronze. The energy corresponding to the compressional wave will propagate along the boundary, as discussed above. Therefore there is no contribution to the reflection series from the term R_{sp}, and nothing is lost by ignoring it.

Further, a great deal of experimental evidence indicates that shear waves in rubber are highly damped, so that they are not observed in the reflection series for reasonable thicknesses of rubber. The energy represented by terms such as T_{ss}, corresponding to shear waves in rubber generated by shear waves in bronze, is lost to heat. It must be accounted for when calculating the other reflection and transmission coeffecients, but once this is done, its contribution to the reflection series is negligible.

Therefore the model developed above is appropriate to the problem of alternate bronze and rubber layers. It can be extended to the case of several layers in the same way as was done for the case of normal incidence.

One effect not predicted by the model is the location of the emerging pulse of energy. For the normal incidence case, this point is just the entrance point, but for beams at an angle the emergence point is displaced by some amount. This distance can readily be calculated: it is just twice the layer thickness times the tangent of the angle the relevant ray path makes with the normal. Each transit of each layer contributes this quantity to the overall displacement of the exit point, and therefore the contributions of all transits of all layers must be added to get the total displacement.

The angle of the ray path is generally different from layer to layer, and from mode to mode within a layer. It can be calculated by Snell's law. If Θi is the angle made by the ray in question with respect to the normal, and v_i the velocity of the phase in the i-th layer, then

$$V = v_i/\sin(\Theta_i) \qquad 1.1$$

holds for all layers. V is called the phase velocity, and is a constant throughout the layered structure.

Having found the formalism by which the arrival times and amplitudes may be calculated for the off-normal incidence case, the reflection and transmission coefficients referred to above are calculated. In [2] the potentials ϕ and ψ are introduced whose derivatives give rise to compressional and shear waves as follows:

$$u = \partial\phi/\partial x - \partial\psi/\partial z$$
$$w = \partial\phi/\partial z + \partial\psi/\partial x \qquad 1.2$$

where u and w are displacements in x and z, respectively. If the form

$$u = v_o e^{i\omega \cdot x}$$

is assumed, the derivatives of equation 1.2 are equivalent to multiplication by $i\omega/v$.

The equations for continuity of displacement and stress at the boundary take the form

$$\begin{aligned} A_1 + A_1' &= M_{13} A_2 + M_{14} B_2 \\ B_1 - B_1' &= M_{23} A_2 + M_{24} B_2 \\ A_1 - A_1' &= M_{33} A_2 + M_{34} B_2 \\ B_1 + B_1' &= M_{43} A_2 + M_{44} B_2 \end{aligned} \qquad 1.3$$

Here A refers to the amplitude of the compressional potential and B to that of the shear potential. The subscript 1 refers to the upper layer, and 2 to the lower layer. Reflected waves (present in the upper layer only) are denoted by a prime sign ('). The coefficients M_{ij} are functions of the material properties only, and are detailed in [2].

Only one incident wave at a time need be considered in the upper layer. In the case above, only a shear wave is incident there. Then the incident p wave amplitude A_1 is zero, and B_1 is the amplitude of the incident wave potential. We divide each of the Equations 1.3 by B_1, and make the following identifications:

$$A_1'/B_1 = r_{sp}$$

$$A_2/B_1 = t_{sp}$$

$$B_1'/B_1 = r_{ss}$$

$$B_2/B_1 = t_{ss}$$

Then the equations 1.3 can be written in matrix notation as

$$\begin{bmatrix} 0 \\ 1 \\ 0 \\ 1 \end{bmatrix} = \begin{bmatrix} -1 & 0 & M_{13} & M_{14} \\ 0 & 1 & M_{23} & M_{24} \\ 1 & 0 & M_{33} & M_{34} \\ 0 & -1 & M_{43} & M_{44} \end{bmatrix} \begin{bmatrix} r_{sp} \\ r_{ss} \\ t_{sp} \\ t_{ss} \end{bmatrix} \qquad 1.4$$

Denoting the square matrix of coefficients on the right by H, the solution for the desired reflection and transmission coefficients is

$$\begin{bmatrix} r_{sp} \\ r_{ss} \\ t_{sp} \\ t_{ss} \end{bmatrix} = H^{-1} \begin{bmatrix} 0 \\ 1 \\ 0 \\ 1 \end{bmatrix} \qquad 1.5$$

A complex matrix inversion routine is required to evaluate this expresssion on a digital computer.

Finally, to get reflection coefficients, the coefficients given above must be multiplied by an appropriate ratio of velocities. Thus if V_s is the shear velocity in layer 1 and V_p the compressional velocity in layer 2,

$$T_{sp} = t_{sp}\frac{V_p}{V_s}$$

and so on in accordance with equation 1.2.

Figure 1.2 shows the theoretical reflection coefficients for the case of a shear wave in bronze incident on a rubber half space, as a function of the shear wave angle in bronze. Amplitudes are shown in Figure 1.2a, and the phase in Figure 1.2b.

Figure 1.2a does not give all the information required to pick the optimum inspection angle. This is because the phase shift given in Figure 1.2b also affects the amplitude in the time domain. To see how it does so, take the incident pulse to be an impulse, given in the time domain by

$$(t) = \int_{-\infty}^{\infty} e^{i\omega t}\, d\omega \qquad 1.6$$

Then a reflected pulse f(t), where the reflection coefficient is $r\, e^{i\Theta}$, is given by

$$f(t) = r\int_{-\infty}^{\infty} e^{i\omega\left(t+\frac{\Theta}{|\omega|}\right)} d\omega \qquad 1.7$$

The presence of the absolute value of the frequency in the integral is required to make the phase shift correspond to an increase in the time for negative as well as positive frequencies.

This integral can be evaluated, and the resultant pulse is

$$f(t) = r\delta(t)\cos\Theta + (r/2\pi^2 t)\sin\Theta \qquad 1.8$$

It is plotted in Figure 1.3 for several values of phase shift.

This pulse displays noncausal behavior in that it has non-zero amplitude at large negative times, but this is not cause for concern, for the same reasons that it was not in the case of the constant Q model. The assumption of plane wave behavior has been made here which is violated at a low enough frequency (and hence large enough wavelength) for any finite size reflector.

The general properties predicted for f(t) by equation 1.8 have been verified seismically.

The utility of Equation 1.8 is that it may be convolved with the assumed shape of the incident pulse to find the time domain amplitude of the reflected or transmitted pulse. The peak amplitude of this pulse is what is really used for detection.

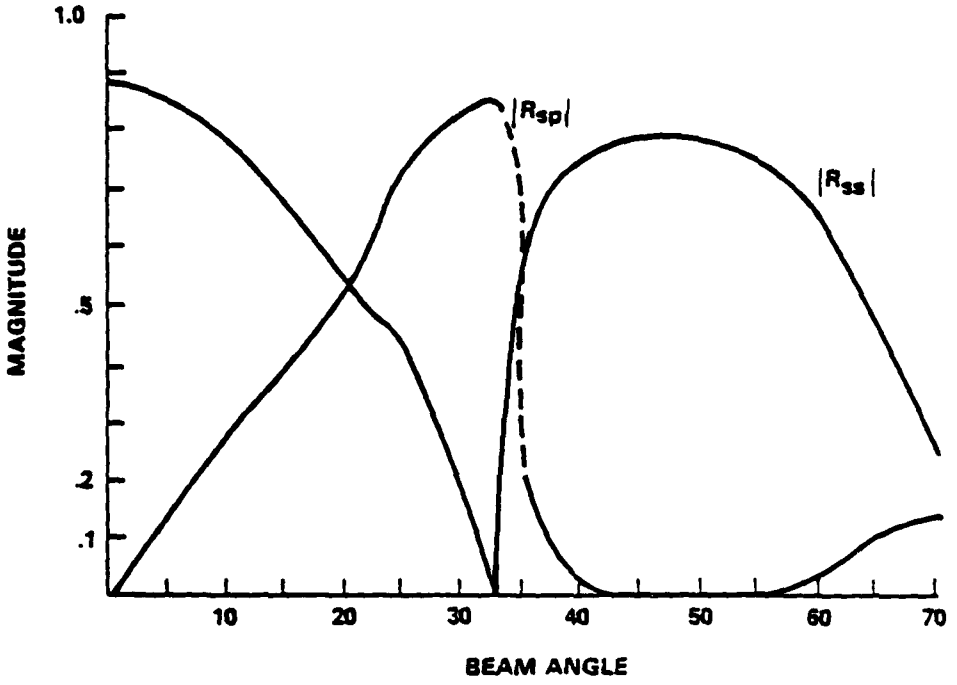

MAGNITUDE OF R_{SP} AND R_{SS} VERSUS ANGLE IN BRONZE

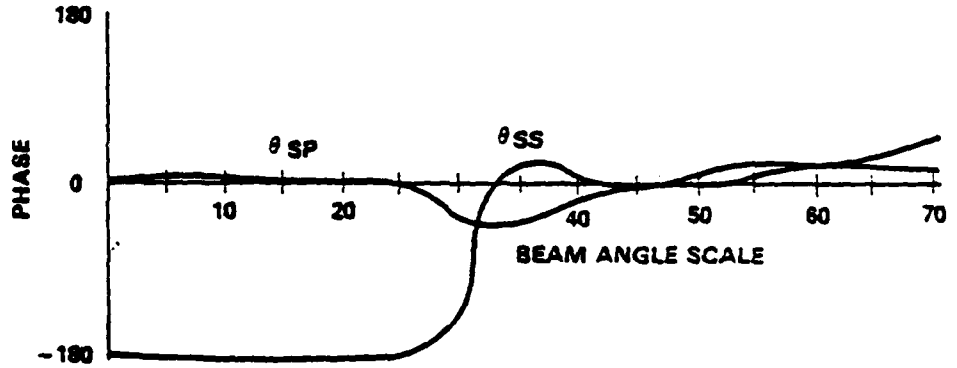

PHASE OF R_{SP} AND R_{SS} VERSUS ANGLE IN BRONZE

Figure 1.2 REFLECTION COEFFICIENTS BRONZE RUBBER INTERFACE

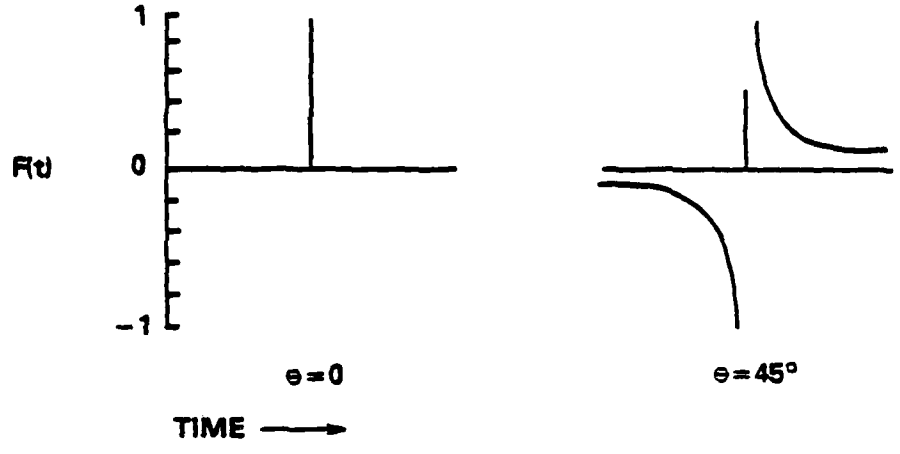

FOR A δ FUNCTION INPUT OUTPUT IS $f(t) = \cos\theta\ \delta(t) + \sin\theta/2\pi^2 t$

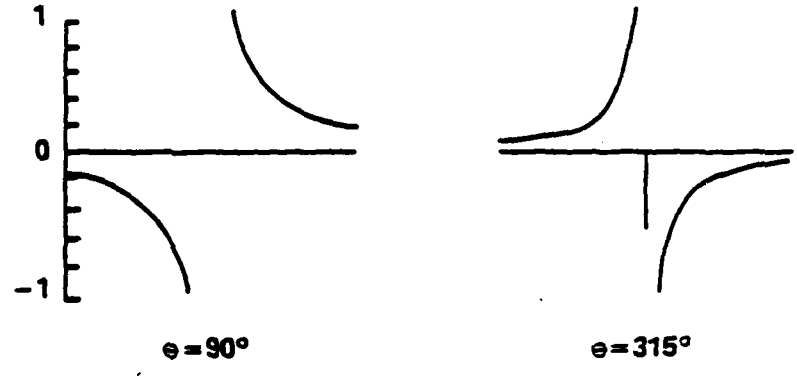

Figure 1.3 EFFECT OF PHASE SHIFT ON WAVEFORM

1.3 COMPUTER IMPLEMENTATION OF ANGLE BEAM MODEL

The computer model developed under Phase 1 was modified to include beam angles off normal. This meant implementing the matrix equation in Equation 1.4 to compute the eight (8) complex reflection and transmission coefficients for the downgoing and upgoing waves at each interface. In addition, the computer program allows the user to vary the beam entry angle over a range of values in incremental steps specified by the user.

1.3.1 Model Inputs

The material characteristics used in the top and bottom half space and in the multilayered specimen are specified. These characteristics include: material thickness (for each layer in the specimen) and density, longitudinal and shear wave velocities, attenuation (in dB/mm) at the frequency with which the specimen will be inspected and the desired mode of propagation in that layer (i.e., whether shear or longitudinal). The user also specifies the sampling interval of the reflection series and the signal length (in number of points).

1.3.2 Model Output

The model generates the complex reflection series as a function of time. The time axis should also be interpreted as travel path, by multiplying by the phase velocity (equation 1.1). This remains constant for all layers and so a linear transformation of the time axis will yield the transducer separation. Along with the real and imaginary parts of the reflection series, the program also generates its magnitude. If the user specifies varying beam angle, the output will compute the complex and magnitude series for each of the entry angles. The reflection series will consist of impulses whose magnitude, phase and location are computed by the model. This is the impulse response of the multilayered specimen. The output for a specific transducer-receiver pair can be obtained by convolving the impulse response of the pair with the reflection series.

1.3.3 Simulated Reflection Series

Figure 1.4 shows the magnitude reflection series for a bronze-epoxy-aluminum multilayered specimen; the epoxy layer has been specified to be nominally 0.8 mm thick. The beam angles are also indicated in the figure. The top and bottom half spaces are both air.

The decaying magnitude of the (1,0,0), (2,0,0) and (3,0,0) responses, which are located at 1.25, 2.50 and 3.75 μs, is evident. The first return from the bottom of aluminum occurs at about 6.0 μs.

Convolution of the complex reflection series with a 5MHZ transducer-receiver pair, designed for 32° shear wave in bronze is shown in Figure 1.5. Notice that the responses which could be clearly discerned in Figure 1.4 are "smeared" by the transducer-receiver impulse response.

It can be seen, thus, that the limiting factor in discerning the individual returns is the response of the transducer-receiver pair. To improve resolution,

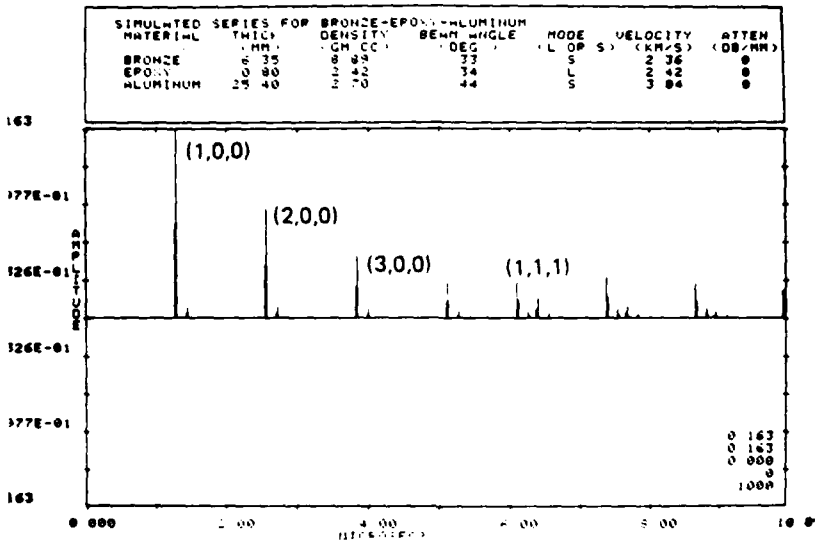

Figure 1.4. SIMULATED REFLECTION SERIES FOR BRONZE-EPOXY-ALUMINUM

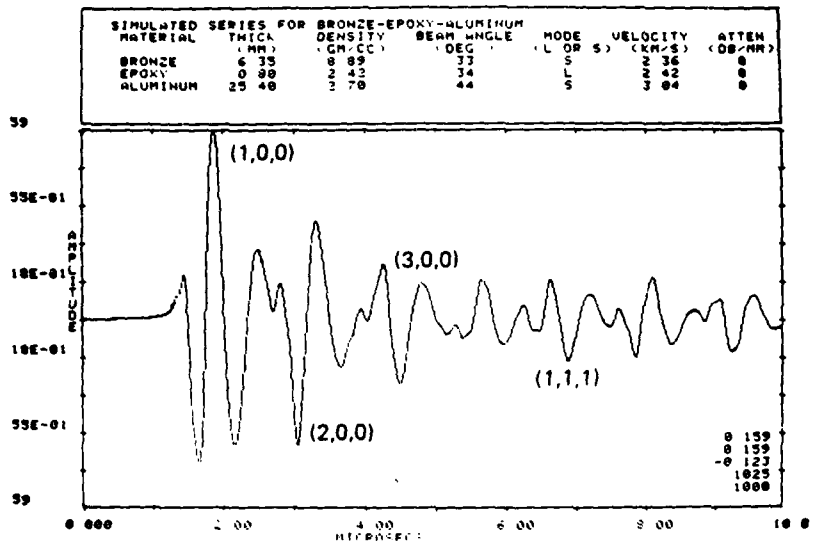

Figure 1.5. SIMULATED REFLECTION SERIES FOR BRONZE- EPOXY-ALUMINUM WITH 5 MHZ TRANSDUCER

signal processing methods -- such as deconvolution or cepstral methods-- must be used.

ANGLE BEAM MODEL VALIDATION

2.1 INTRODUCTION

Model validation was performed by comparing four different aspects of the simulated series with actual data. These four were: time of travel in each layer, mode of propagation, the amplitude, and finally the phase of the response from different interfaces. To reiterate, the model predicts that reverberations within each layer will be a rotational phasor whose amplitude and phase vary by a constant amount, unlike the normal-incident case where the phase is unaffected. The model was validated by comparing ultrasonic data from a bronze-epoxy-aluminum structure with its simulated series. The structure was chosen because both bronze and aluminum do not significantly attenuate the acoustic signal.

2.2 ULTRASONIC DATA COLLECTION

The bronze-aluminum specimen were, respectively, 6.35 mm and 25.40 mm thick. In between a layer of epoxy was used to hold the specimens. This layer was nominally 1.00 mm thick. Both the bronze and aluminum layers were machine finished.

Figure 2.1 shows a schematic of the experimental arrangement. A pair of transducers, rated at 5 mHz, whose crystal face was approximately 6.4 mm by 6.4 mm, was mounted on plastic wedges to produce a 45° shear wave beam in aluminum. This translated to aproximately a 33° shear wave in bronze. These two angles were beyond critical for longitudinal waves in both materials, insuring that the model output could be compared with the actual data.

A Metrotek pulser-receiver was used in pitch-catch mode with the return signal displayed on a Tektronix T7854 sampling scope. The instrument had a dynamic range of 10 bits and 1024 words of memory. The sampling rate was adjustable and, for the validation study, was set at 102.4 MHZ to provide good resolution. The data were then transferred to an HP-9825 minicomputer and finally to computer-compatible magnetic tapes for analysis.

2.3 MODEL VALIDATION

As indicated previously four aspects of the multilayered response were compared with actual data for model validation. These were

(i) transit time within each layer
(ii) mode of propagation
(iii) amplitude of interface response
(iv) phase angle of the interface response.

While absolute values could not be compared -- because of the unknown delay and magnitude and phase response of the transducer pair -- the relative changes with respect to a reference response could be compared for both simulated and actual data.

The actual data that were used for validation consisted of the (3,0,0), (4,0,0), (5,0,0) responses, i.e., those that passed only through the bronze layer

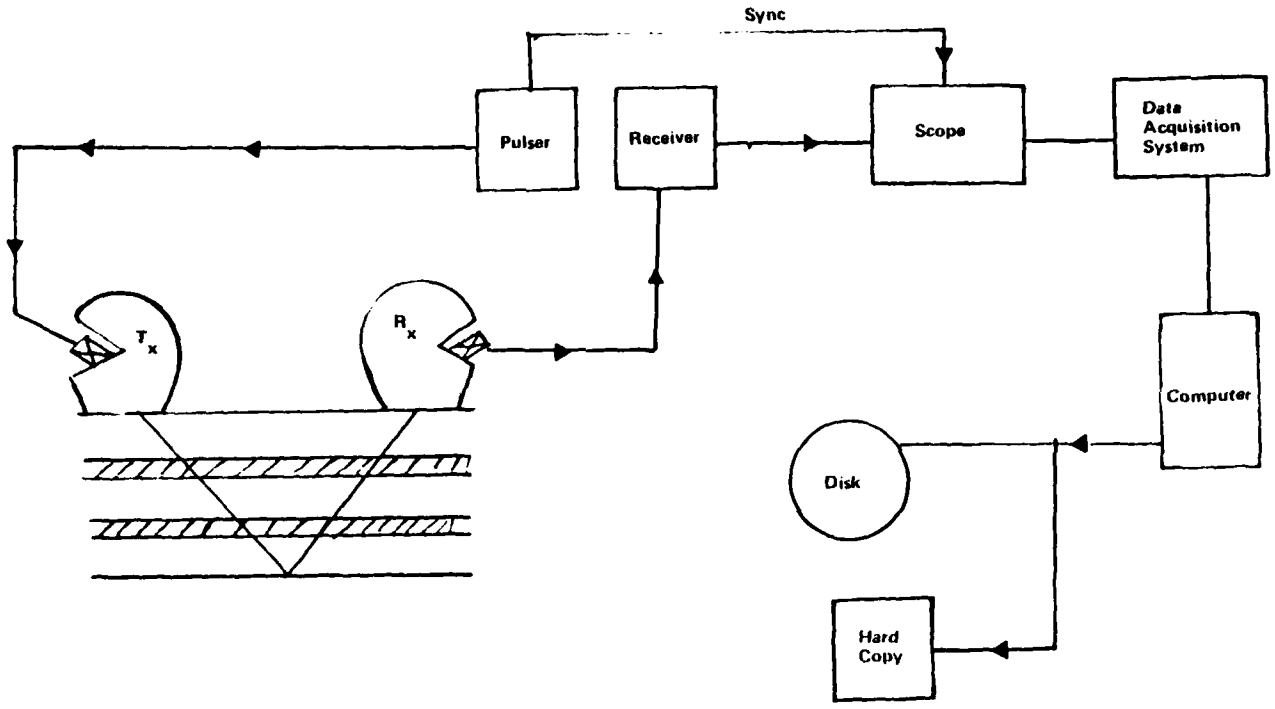

Figure 2.1. SCHEMATIC ARRANGEMENT FOR ULTRASONIC DATA ACQUISITION

three, four and five times, respectively. In addition, the responses from the bottom aluminum layer were also analyzed. These were the (1,1,1), (2,1,1) and (3,1,1) response. The response for each of these paths was obtained by "peaking" the receiver response by moving it to the appropriate location.

2.3.1 Validation of Transit Time and Propagation Mode

Figure 2.2 (a) through 2.2(f) show the individual responses. The delay time of these responses are tabulated below:

Response	System Delay (μs)	Delay in Window (μs)	Total Delay (μs)
(3,0,0)	25.64	4.58	30.22
(4,0.0)	32.39	4.51	36.90
(5,0,0)	39.14	4.55	43.69
(1,1,1)	37.40	2.75	40.15
(2,1,1)	42.62	4.04	46.66
(3,1,1)	49.49	3.75	53.24

Table 2.1: Time Delay Measurements

The average difference between the (3, 0, 0), (4, 0, 0), and (5, 0, 0), and between the (1, 1, 1), (2, 1, 1), and (3, 1, 1) is 6.64 μs which is the bronze transit time. The theoretically computed transit time for a 33° shear wave in bronze 6.35 mm thick is (refer to table in Figure 1.4)

$$t_{Bronze} = \frac{2 \times 6.35}{2.2\cos(33)} = 6.58\mu s$$

This compares favorably with the actual measured value.

From the data Table 2.1 the delay within the transducer wedges can be computed from the (3,0,0) response, by subtracting from it three times the average bronze transit time (6.64 μs). This delay is 30.22 - 3x6.64 = 10.30 μs. Subtracting the wedge delay and the average bronze time from the (1,1,1) transit time gives the combined epoxy-aluminum transit time: this time is 40.15 - 10.30 -6.64 = 23.21 μs. Ignoring the time within the epoxy layer, the theoretical transit time within aluminum for a shear wave at 44° is (refer to table in Figure 1.4)

$$t_{alum.} = \frac{2 \times 25.4}{3.04 \times \cos(44)} = 23.23\ \mu s$$

which is a close match to the actual measured value of 23.21 μs.

2.3.2 Validation of Signal Magnitude

Validation of the signal magnitudes with that predicted was accomplished by first computing the power spectrum of the signals in Figures 2.2(a) through (f) and then measuring the power in a band of frequencies around the center

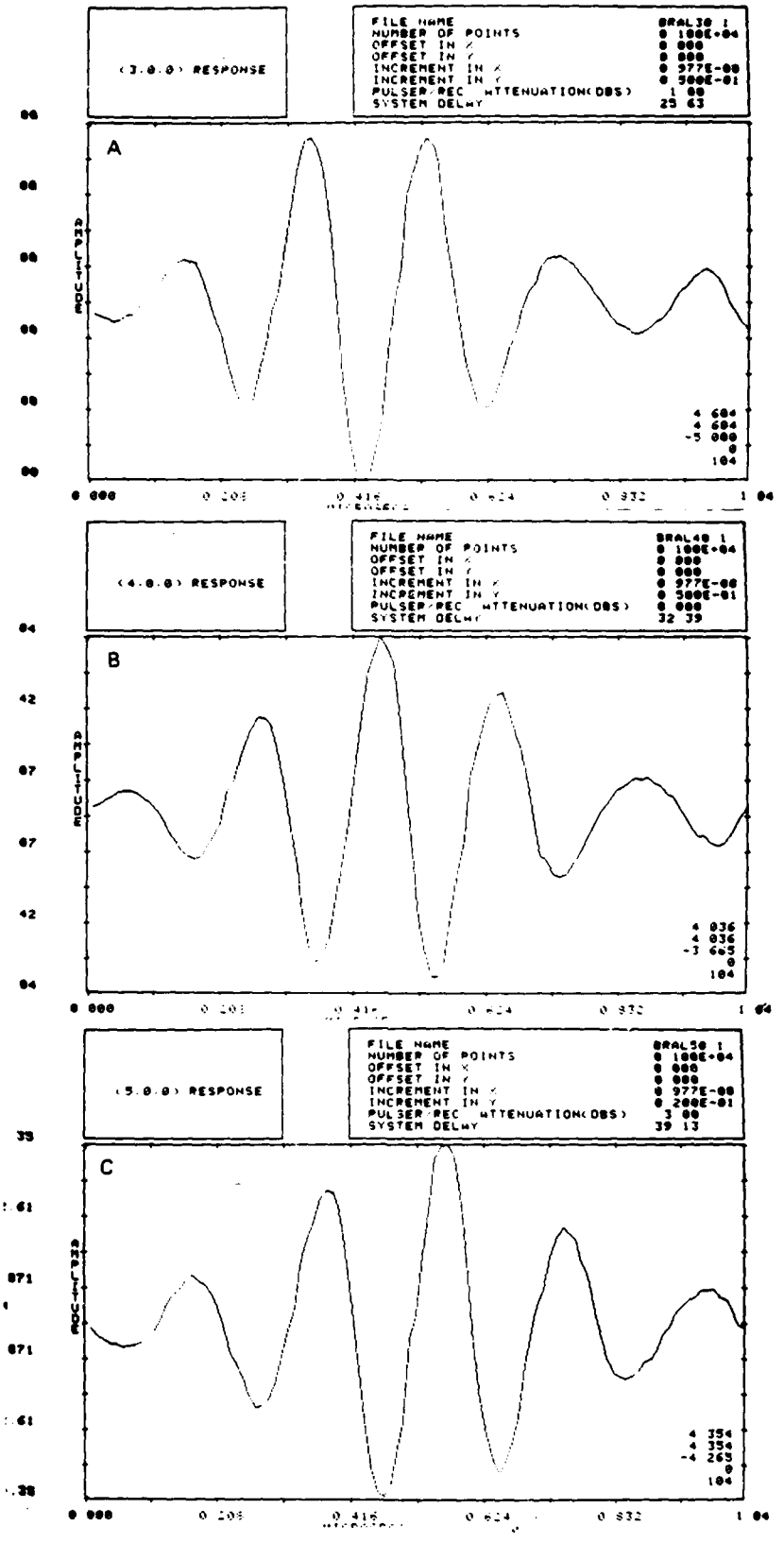

Figure 2.2. DIGITAL WAVEFORMS USED IN MODEL VALIDATION

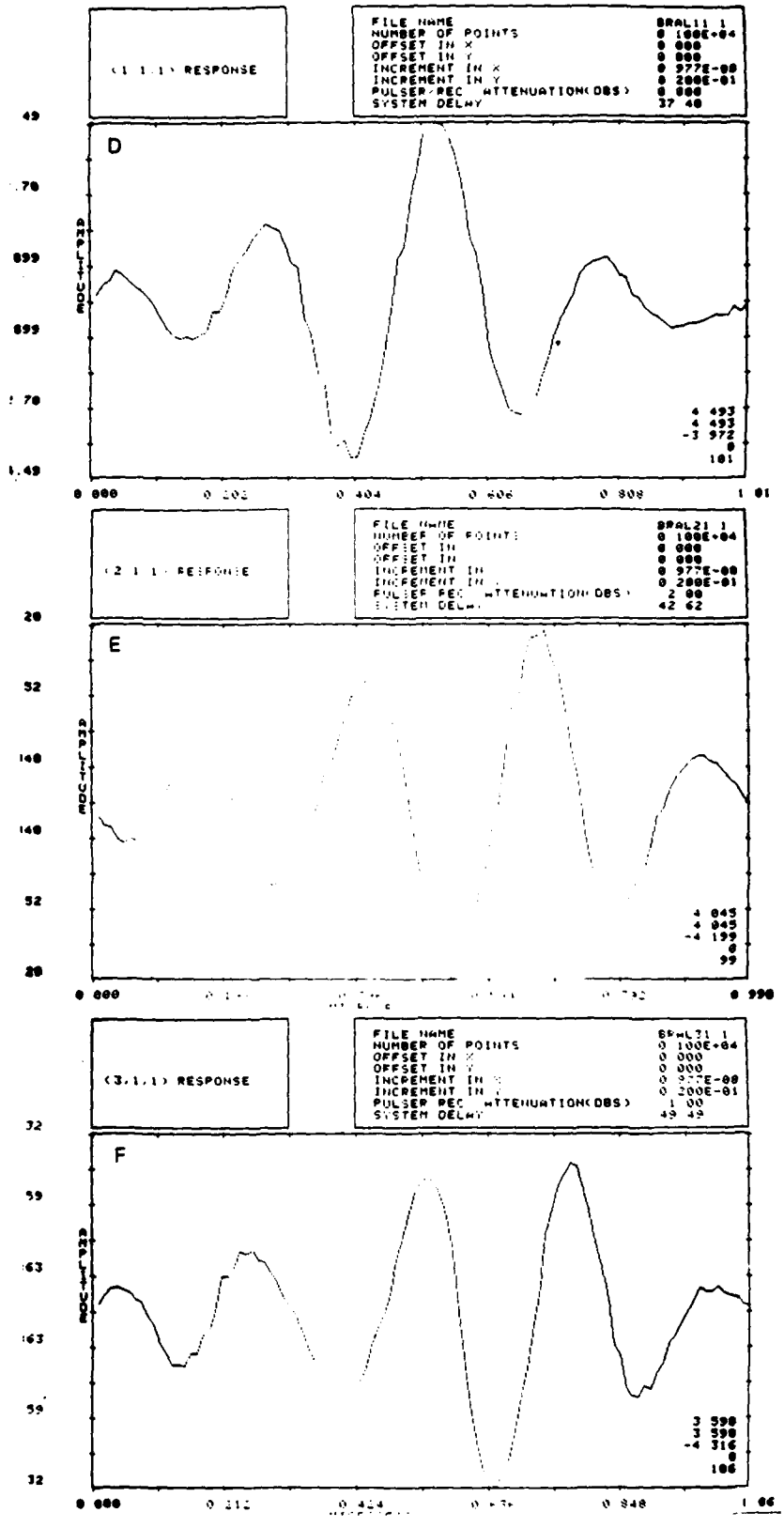

Figure 2.2. DIGITAL WAVEFORMS USED IN MODEL VALIDATION CONT'D

frequency. Since the receiver amplifier had a variable attenuation feature and the oscilloscope's voltage sensitivity was adjusted for maximum dynamic range, the power computed had to be standardized to a fixed attenuation and sensitivity setting. Peak amplitudes could not be used for this purpose due to the effects of the phase shift introduced by the complex reflection and transmission coefficients.

Figures 2.3(a), through (f) show the log magnitude spectrum of the six responses shown in Figure 2.2. It can be seen that the responses from the bronze-epoxy interface are all centered around 5 MHZ. The responses from aluminum, however, show a peak shift toward a lower frequency, i.e., about 3.8 MHZ. This is because of attenuation within epoxy or aluminum or both. Therefore, to make valid comparisons between model output and actual data, the returns from the aluminum layer had to be compensated according to a constant Q model [see reference 1].

The reverberation within bronze, however, did not have to be compensated. Table 2.2 lists the average measured amplitude of the magnitude spectrum about + 0.4 MHZ of the peak power for the (3,0,0), (4,0,0) and (5,0,0) responses. Also indicated are the receiver amplifier attenuation, data acquisition system sensitivity, and finally the actual voltage and dB change with respect to the (3,0,0) reponse.

Response	Average Amplitude (units)	Amplifier Attenuation (dB)	Voltage Sensitivity (v/div)	Actual Voltage	dB Change
(3,0,0)	10.855	1	0.05	0.6090	0
(4,0,0)	8.944	0	0.05	0.4472	-2.7
(5,0,0)	10.753	3	0.02	0.3038	-6.0

Table 2.2: Amplitude Measurements for Bronze Reverberation

The average decay per round trip path in bronze is 2.9dB (2.7 + 6.0/2 = 2.9). The response predicted by the model is enumerated in Table 2.3. The beam angles in bronze and aluminum are, respectively, 33° and 44°. The acoustic parameters used are listed in the table in Figure 1.4. The half space on either side is air.

Response	Amplitude ($x10^6$)	dB Change	Phase [(3,0,0) reference]
(3,0,0)	25.999	0	0°
(4,0,0)	17.379	-3.5	-133
(5,0,0)	11.617	-7.0	94
(1,1,1)	12.266	-6.5	-65
(2,1,1)	16.396	-4.0	162
(3,1,1)	14.438	-4.0	29

Table 2.3: Model-Predicted Amplitude and Phase Response.

It can be seen from Table 2.3 that the rate of decay predicted for the bronze reverberations is 3.5 dB per round trip compared to an average of 2.9 dB

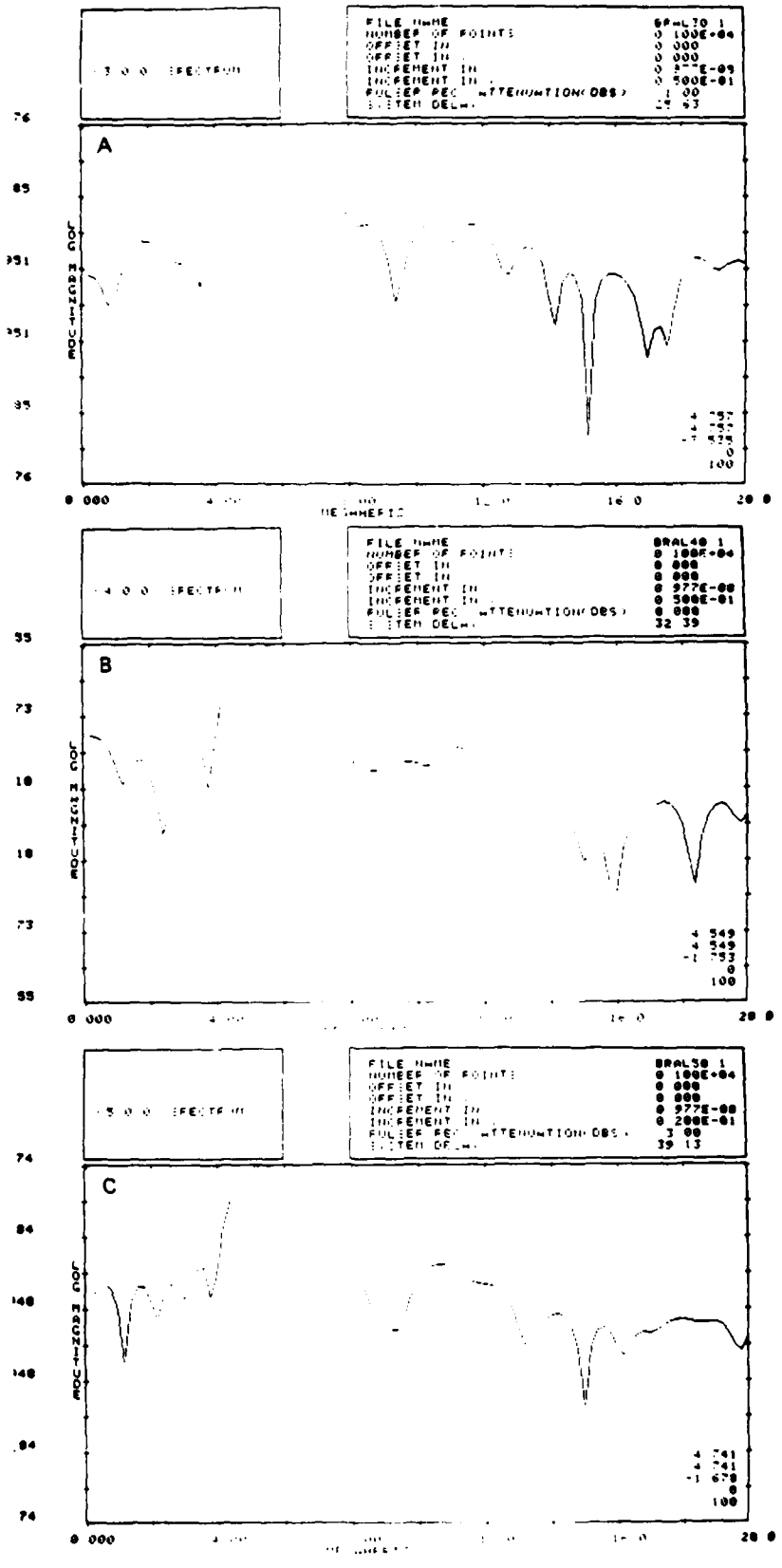

Figure 2.3. MAGNITUDE SPECTRUM OF WAVEFORM USED IN MODEL VALIDATION

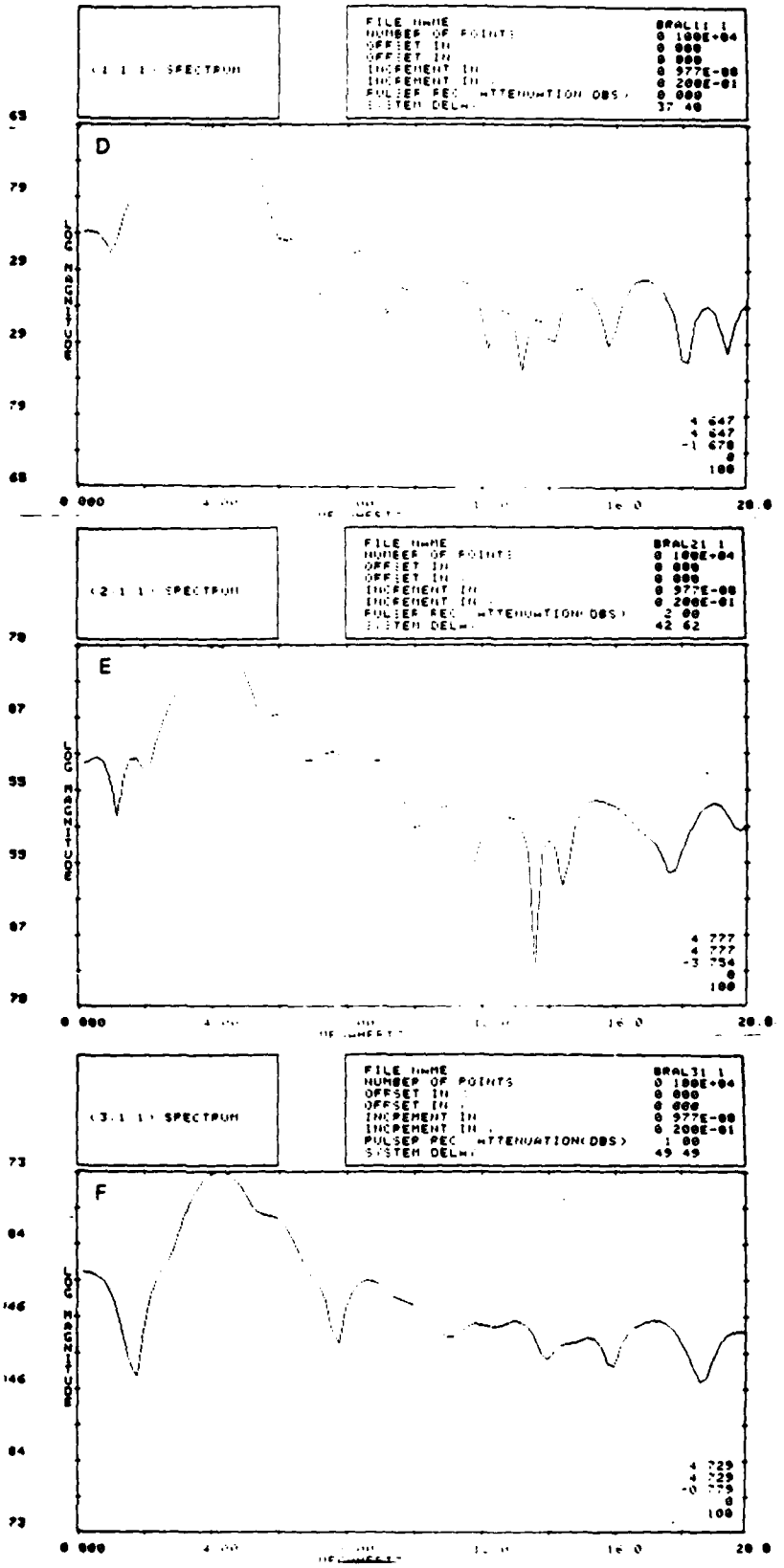

Figure 2.3. MAGNITUDE SPECTRUM OF WAVEFORM USED IN MODEL VALIDATION CONT'D

measured. The discrepancy of 0.6 dB may be due to improper choice of acoustic constants, but from a practical standpoint the discrepancy is well within experimental errors.

To validate the amplitudes of the aluminum returns, the magnitude spectrum of these responses were compensated for frequency-dependent attenuation. Figure 2.4 shows the log magnitude spectra and their difference for a (3,0,0) and (1,1,1) path. Notice that the (3,0,0) response peaks at 5.0 MHZ, while the (1,1,1) peaks at 4.0 MHZ. The difference of the log spectra appears to be linear, verifying that there exists linear, frequency-dependent attenuation. The slope of the difference is 16.5 dB/MHZ. The compensating factors at different frequencies are therefore:

Frequency(MHZ)	Compensating Factor (dB)	Amplitude Ratio
4.0	-10.0	0.32
4.5	- 1.8	0.81
5.0	+ 6.5	2.11
5.5	+14.8	5.50
6.0	+23.0	14.13

The amplitudes of the aluminum returns at different frequencies should be modified according to the appropriate value listed in the table.

The measured and compensated amplitudes from the frequency response of the (1,1,1), (2,1,1) and (3,1,1) paths are listed.

Response	Compensated Average Amplitude (units)	Amplifier Attenuation (dB)	Voltage Sensitivity (v/div)	Actual Voltage (v)	dB Change (relative to 3,0,0)
(1,1,1)	12.192	0	0.02	0.2438	-7.9
(2,1,1)	11.055	2	0.02	0.2783	-6.8
(3,1,1)	16.471	1	0.02	0.3696	-4.3

Table 2.4: Response of the Bronze Aluminum Paths.

The dB change shown in Table 2.4 should be compared to that predicted in Table 2.3. The measured and predicted for the (1,1,1) response, with (3,0,0) response as reference, are -7.9 and -6.5 dB, respectively; while for the (2,1,1) response they are -6.8 and -4.0 and for the (3,1,1) response they are -4.3 and -4.0. The average discrepancy is approximately 1.5 dB, which could be due to inadequate compensation or due to experimental error.

2.3.3 Validation of Signal Phase

The phase spectra of the different responses were computed using the FFT algorithm. Since the (3,0,0), (4,0,0) and (5,0,0) responses were different spectrally from (1,1,1), (2,1,1) and (3,1,1) -- because of frequency-dependent attenuation in aluminum -- comparing the former set with the latter set could

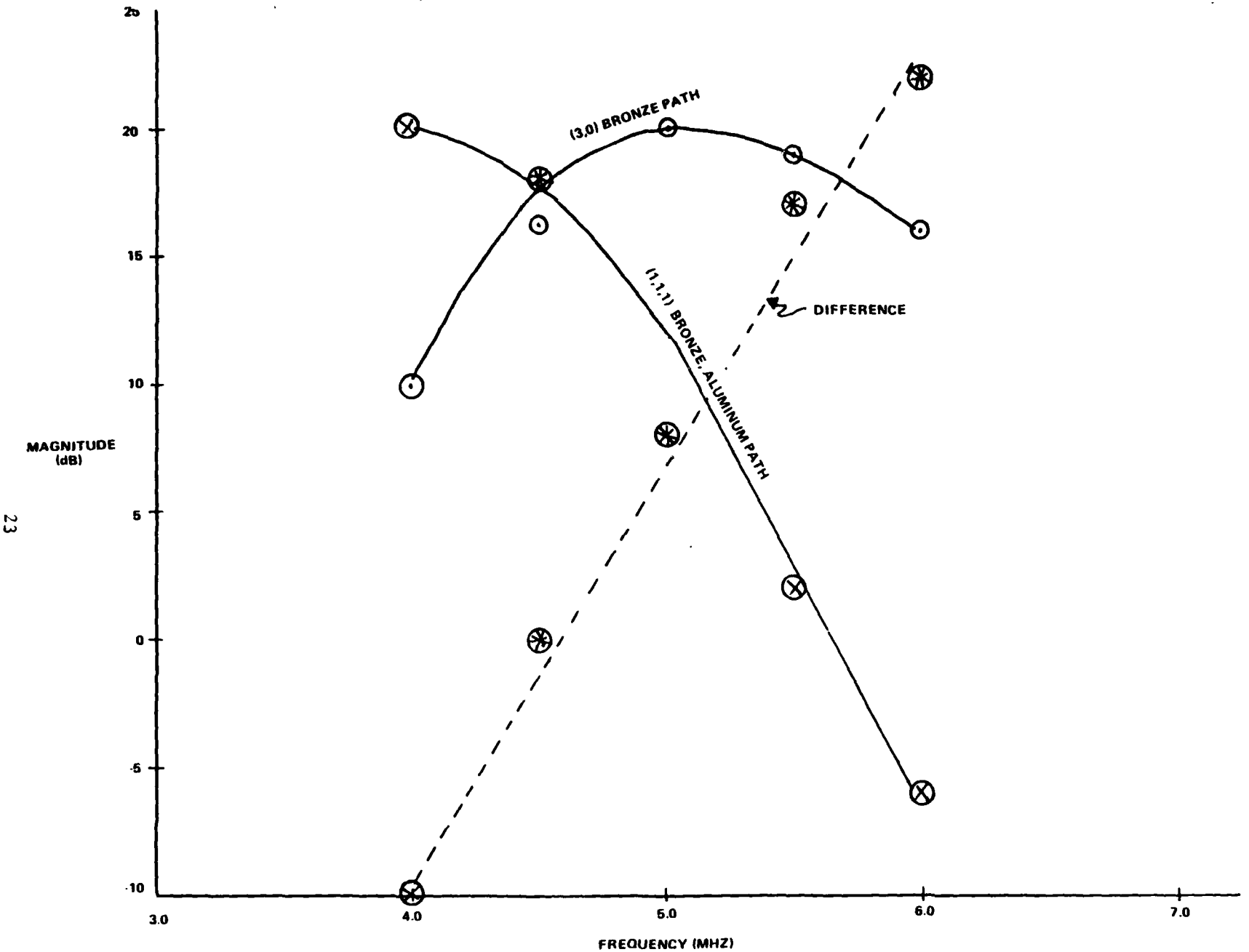

Figure 2.4. MAGNITUDE SPECTRA AND DIFFERENCE OF BRONZE AND ALUMINUM RESPONSE

only be accomplished over a frequency range common to the two; however comparisons within each set could be made over the frequency range where the power was considerable. For the first set it was ± 0.4 MHZ, centered about 5.2 MHZ, while for the latter set it was also ± 0.4 MHZ, centered around 4 MHZ.

The phase difference for the first set is tabulated below and the average phase difference computed.

	Phase Difference (Degrees)	
Frequency (MHz)	(3,0,0) and (4,0,0)	(4,0,0) and (5,0,0)
4.8	-150	-172
5.0	-148	-170
5.2	-147	-168
5.4	-145	-166
5.6	-143	-162
Average Difference:	-147±3	-168±4

The measured phase shift at different frequencies between the (1,1,1) and (2,1,1), which is indicative of the phase shift due to one bronze transit path, were:

Frequency	Phase Difference (1,1,1) and (2,1,1)
3.6	-177
3.8	-172
4.0	-169
4.2	-166
4.4	-162
Average Difference:	-169 ± 6

The overall average phase shift measured for one bronze reverberation is therefore -161° (i.e., (-147)+(-118)+(-169)/3).

The model predicted phase difference for one bronze reverberation is -133° for a 33° shear wave beam in bronze (see Table 2.3). This phase difference compares well with that measured.

The measured phase difference between (3,0,0) and (1,1,1) for two frequencies where the magnitude spectra show overlap is:

Frequency	Phase Difference (3,0,0) and (1,1,1)	Phase Difference (3,0,0) and (2,1,1)
4.6	-34	167
4.8	-35	171
Average Difference:	-35	169

The average difference predicted by the model for the (3,0,0) and (1,1,1) difference is -65, and between (3,0,0) and (2,1,1) it is +162 (see Table 2.3). Again this discrepancy between the measured and predicted could be due to improper choice of acoustic parameters especially in the poorly understood epoxy layer and due to experimental error.

2.4 SUMMARY OF VALIDATION RESULTS

Table 2.5 gives an overall comparison of the measured and predicted amplitude and phase response, with the (3,0,0) response taken to be unit magnitude and zero phase.

Response	Amplitude (dB)		Phase (degrees)	
	Experiment	Theory	Experiment	Theory
(4,0,0)	-3.0	-3.5	-164	-133
(5,0,0)	-6.0	-7.0	-322	-266
(1,1,1)	-7.9	-6.5	-35°	-64°
(2,1,1)	-6.8	-4.0	+169	+162
(3,1,1)	-4.3	-4.0	+8°	+29°

Table 2.5. Comparison Between Experimental Measurements and Theoretical Results

The comparison is illustrated in Figure 2.5. It can be seen that both magnitude and phase compare satisfactorily.

Validating the model allows one to design the optimum beam angle for inspecting bronze-rubber specimens. The choice of angle would optimize the response in the presence of a flaw. The angle would be selected so that there is a maximum phase shift in the presence and absence of a flaw.

The rest of the report details the experimental techniques including selection of the optimum beam angle and signal processing methods for inspecting bronze-rubber multilayered parts.

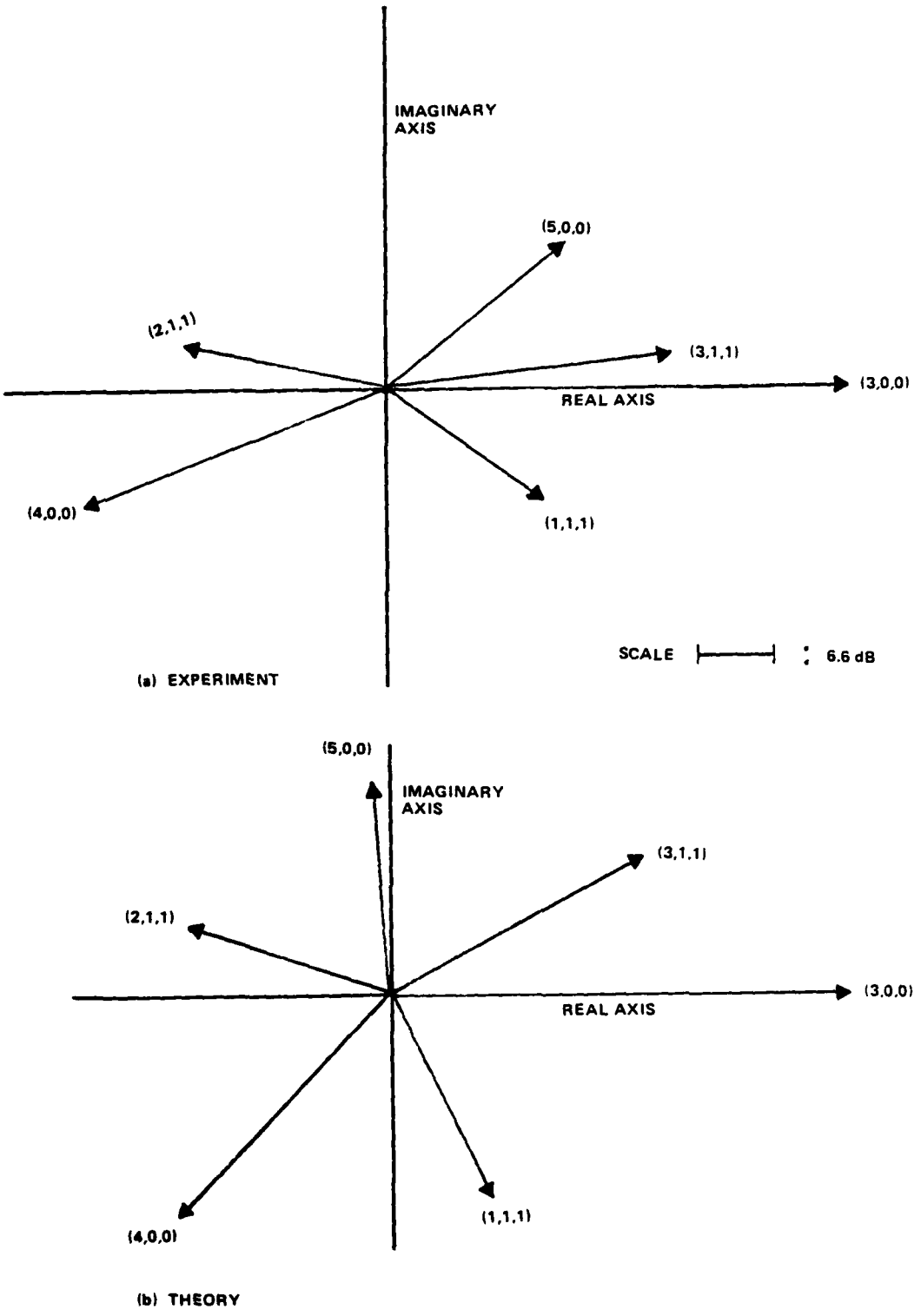

Figure 2.5. PHASOR COMPARISON BETWEEN EXPERIMENT AND THEORY FOR SIX RESPONSES FROM A BRONZE-EPOXY-ALUMINUM STRUCTURES

SELECTION OF INSPECTION CONFIGURATION FOR BRONZE RUBBER SPECIMENS

3.1 INTRODUCTION

The model was applied to the structure of bronze and rubber layers of interest to the Navy. Table 3.1 shows the parameters of bronze, rubber and epoxy relevant to the problem.

	V_p (mm/ s)	V_s	Density (gm/cc)	Q_p	Q_s	Thickness (mm)
Bronze	4.85	2.20	8.9			3.175
Epoxy	2.45	--	--	--	--	1.000
Rubber	2.20	1.05	1.37	10	*	6.35

*Too small to measure

Table 3.1 Acoustic parameters for Bronze and Rubber

In order to simplify the problem it was decided to inspect beyond the critical angle (27°) in bronze. Then no longitudinal wave is present in bronze. Due to the low Q of rubber in the shear mode, it seemed unlikely that shear waves through these layers would be important and none were ever observed. Under these circumstances the restriction inherent in the model, to only one kind of wave per layer, is unimportant. Only shear waves in each bronze layer, and compressional waves in each rubber layer, need to be considered.

The parameters of the epoxy layer are not so well known as those of the bronze and rubber layers. Even the epoxy thickness is known only approximately. However, the epoxy layer is expected to be so thin (.010") that attenuation should be negligible unless the epoxy Q is exceptionally low. Therefore Q in epoxy was assumed to be infinite.

Both compressional and shear waves can propagate in epoxy at these angles, a situation beyond the ability of the current model to deal with. However, the epoxy transit time for either phase is so small (0.10μs) compared to a period at typical ultrasonic frequencies (1.0 - 0.2 μsec) that arrival times of phases which have propagated through the epoxy will be substantially independent of which phase carries the energy there.

Since Q for shear waves is usually lower than that for compressional waves, and since the velocity enters into equation for the attenuation in such a way that lower velocity results in greater attenuation even for constant Q, it was assumed that longitudinal waves are more important in the epoxy layer than are shear waves. This assumption is borne out by the agreement between theory and experiment described in Chapter 2 concerning the bronze-epoxy-aluminum results, where the epoxy shear waves were ignored. They will also be ignored in the bronze-epoxy rubber structure.

3.2 INSPECTION ANGLE

The optimum inspection angle for this structure was found by calculating

the reflection series at various angles for a structure with a defect at the bottom of the first rubber layer and one without a defect. The best angle was chosen on the basis of comparisons between these reflection series.

Figure 3.1a and 3.1b represent reflection series for a shear wave angle of 28° in bronze, for a bronze-epoxy-rubber-epoxy-bronze structure, and a bronze-epoxy-rubber structure, respectively. The first structure represents an unflawed specimen, as far as the second epoxy layer is concerned. The second is a reasonable approximation to a lack-of-epoxy condition at the second epoxy layer, although it might be satisfactory for other defects there as well.

The response labeled (1,1,1,1) is the first response diagnostic of conditions at the second epoxy layer, since it follows a direct path to that layer and returns directly to the surface. Other later arrivals from that surface are larger, and then smaller, for reasons explained earlier (Reference 1).

Figures 3.2a and 3.2b represent unflawed and flawed reflection series for an angle of 32° in bronze, and Figures 3.3a and 3.3b are the same for a bronze angle of 36°. A wider range of angles than this was examined in search of the optimum inspection angle, but these three illustrate the results satisfactorally.

It was decided that inspection should be performed by observing a particular response from the second epoxy layer, and that the response and inspection angle should be chosen to simultaneously fulfill two criteria, if possible. First, a large change should occur betwen the flawed and unflawed cases. Second, the response should be detectable in both cases, so that no inferences need be drawn from non-detection of a return.

The reason for the first requirement is obvious: it maximizes the reliability of the flaw-no flaw discrimination. The reason for the second is that lack of detection of a response may be for reasons other than the absence of that response. In the present case, lack of couplant, an unusually thick first epoxy layer, or a high noise level might obscure the return from the second epoxy layer. In this case conclusions about that layer based on this lack of observation would be incorrect. Both the return from the flawed and unflawed layer should be observed.

If both flaw and no-flaw signals are to be as large as possible, discrimination must depend on signal shape. To maximize the change in shape, the phase difference between flaw and no-flaw conditions should be as large as possible; i.e., as near 180° as possible.

The maximum flaw responses could be observed between the (3,0,0) and (4,0,0) responses. This also satisfies the criterion for the minimum physical separation betweeen the pair of transducers that were available. The largest response between the (3,0,0) and (4,0,0) in Figure 3.1 for the unflawed case is the (3,1,1,1); that which has travelled three times within bronze and once each in the epoxy, rubber and second epoxy layer. For the flaw case, the response (3,1,1) is the largest, i.e., that which has no epoxy at the bottom of the rubber layer.

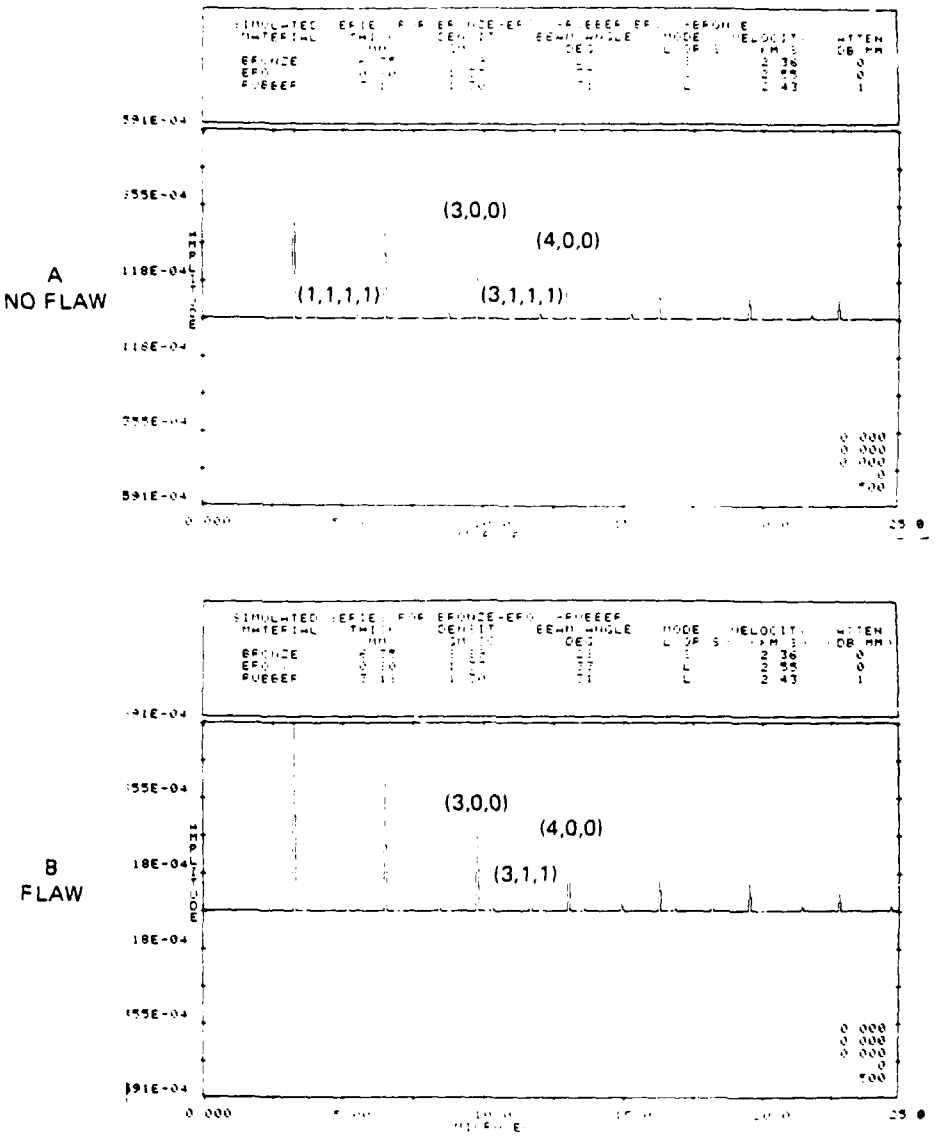

Figure 3.1. SIMULATED BRONZE-EPOXY- RUBBER REFLECTION SERIES FOR 28° SHEAR WAVE IN BRONZE

To satisfy the previous criterion for equally large responses for flawed and unflawed cases, the 28° angle may not be adequate because of the small amplitude of the no flaw signal: it is a negative discriminant and is not of practical value.

For a 32° shear wave (Figure 3.2) however, the magnitudes of the no flaw (3,1,1,1) and flaw signal (3,1,1) are of equal amplitudes and could be discriminated either in time or in the phase characteristics.

At 36° (Figure 3.3), the situation is similar to 32°, perhaps with a small decrease in amplitude of the no flaw signal. At other angles, the ability to detect the small amplitude signals between (3,0,0) and (4,0,0) would be questionable.

So from this an analysis either 32° or 36° appeared to be optimum angles. The final choice was made this on the ability of discriminating between two equally large amplitude signals from their phase behavior. For the reasons detailed below, the 32° shear wave was selected.

Figures 3.4 (a),(b), and (c), show phasor diagrams of the responses of interest in Figures 3.1, 3.2 and 3.3; however, the plots show the phase relationships in addition.

Figure 3.4(a) shows the phasor response of (3,0,0) and (4,0,0) as well as the no-flaw (3,1,1,1) response and the flaw (3.1,1) response for 28° shear wave; the magnitudes are shown in dB's. Although the flaw- and no-flaw phases are 180° apart -- a good condition for separation -- the magnitude of the no flaw response is 20 dB below the (3,0,0) response. This would make detection of this response difficult and the consequent phase measurement inaccurate.

At 32° (Figure 3.4b), however, the two responses are fairly strong, about 10 dB below the (3,0,0) response and the phase difference is approximately 130°, which is almost opposite in phase. So in practical situations the no flaw signals and flaw signals should be easily detectable, and their phases are almost opposite each other, leading to good discrimination capability.

At 36° (Figure 3.4c) the flaw and no-flaw response have dropped about 2 dB from their neighboring (3,0,0) response, but in addition the phasor difference is 110°, a change in 20° from the 32° shear wave case in an unfavorable direction for discrimination.

For the reasons that the magnitude of the flaw and no-flaw signal are relatively large and these phases are almost opposite of each other, the 32° shear wave in bronze was shown to be the optimum angle.

3.3 INSPECTION FREQUENCY

To separate the time-domain (3,1,1) response from the much larger (3,0,0) and (4,0,0) responses, that response should be of the order of the (3,0,0)-(4,0,0) separation time in duration or less. Even after deconvolution or matched filtering, the (3,1,1) response will be on the order of a period or so in duration at the dominant frequency. Therefore the (3,0,0)-(4,0,0) time

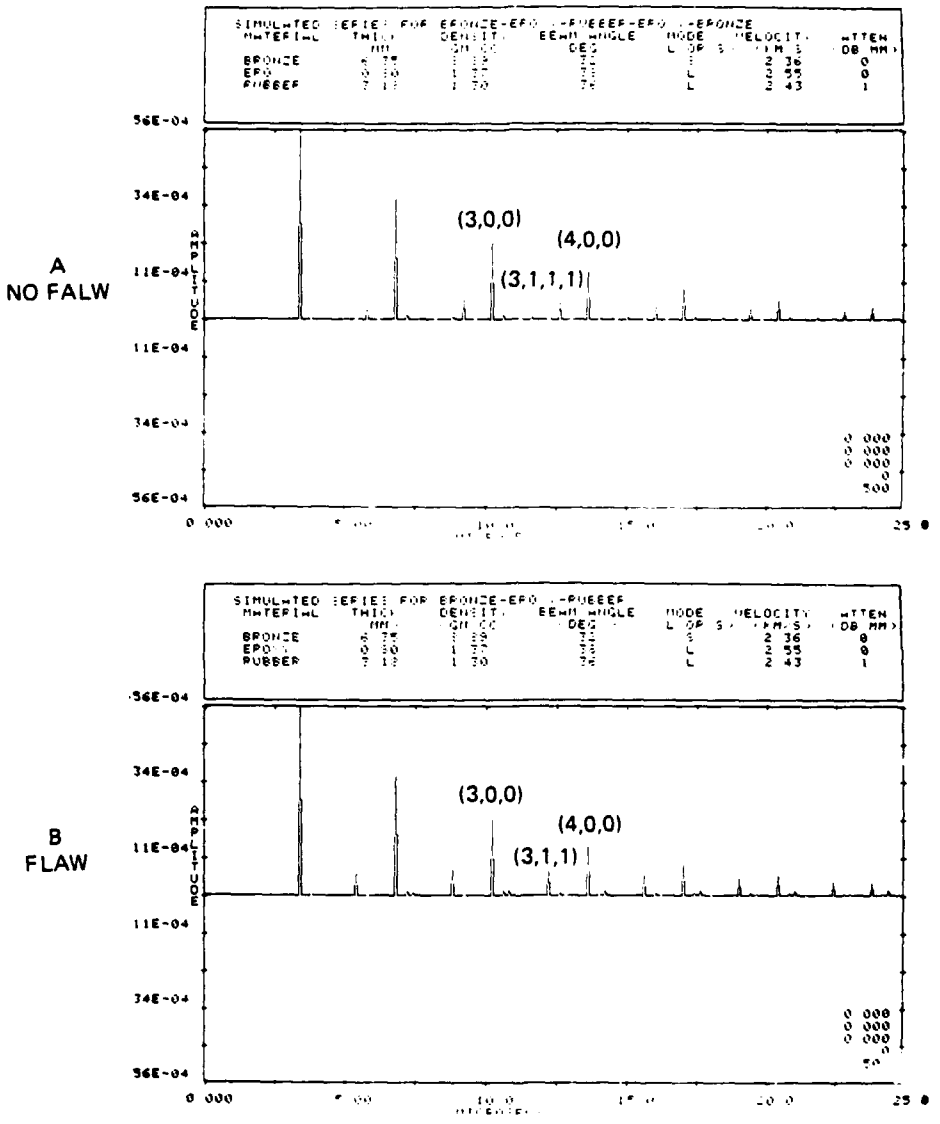

Figure 3.2. SIMULATED BRONZE-EPOXY-RUBBER SERIES FOR 32° SHEAR WAVE IN BRONZE

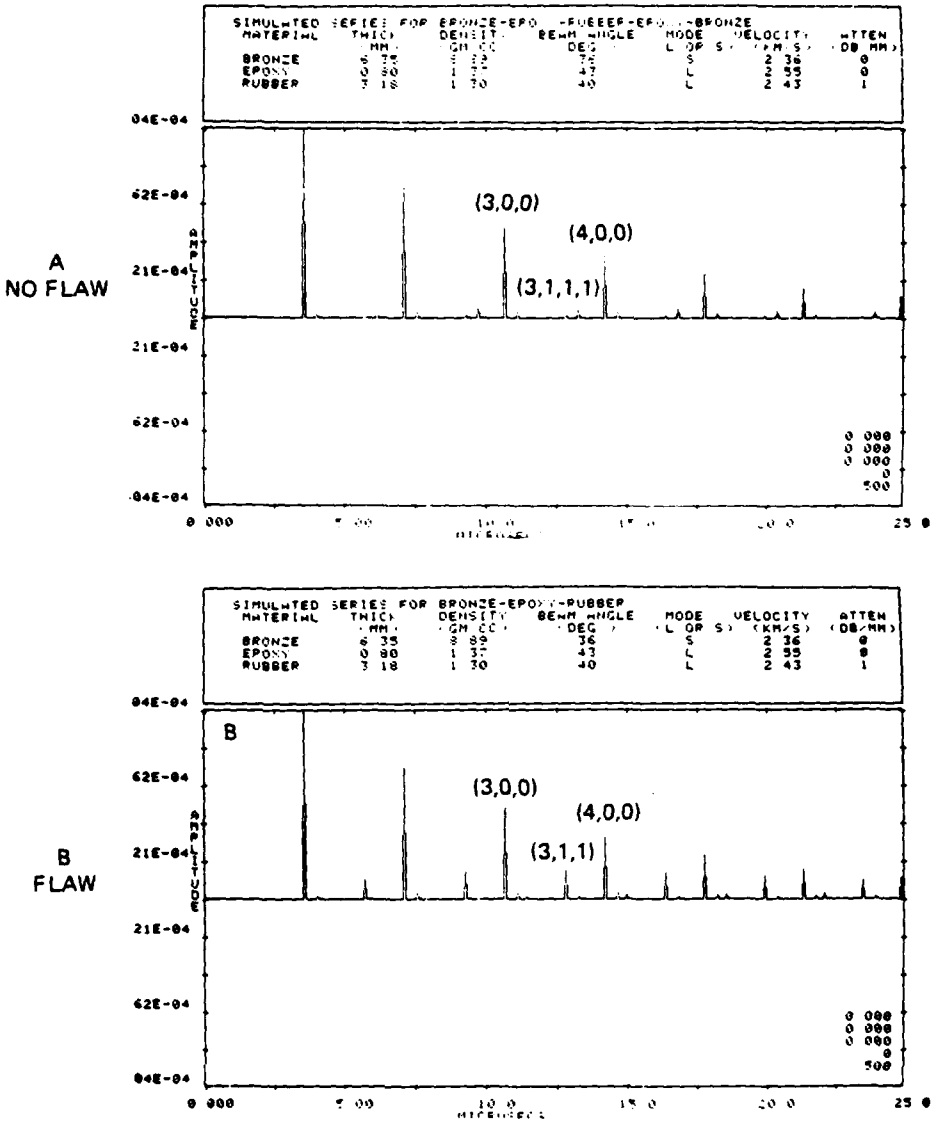

Figure 3.3. SIMULATED BRONZE-EPOXY-RUBBER SERIES FOR 36° SHEAR WAVE IN BRONZE

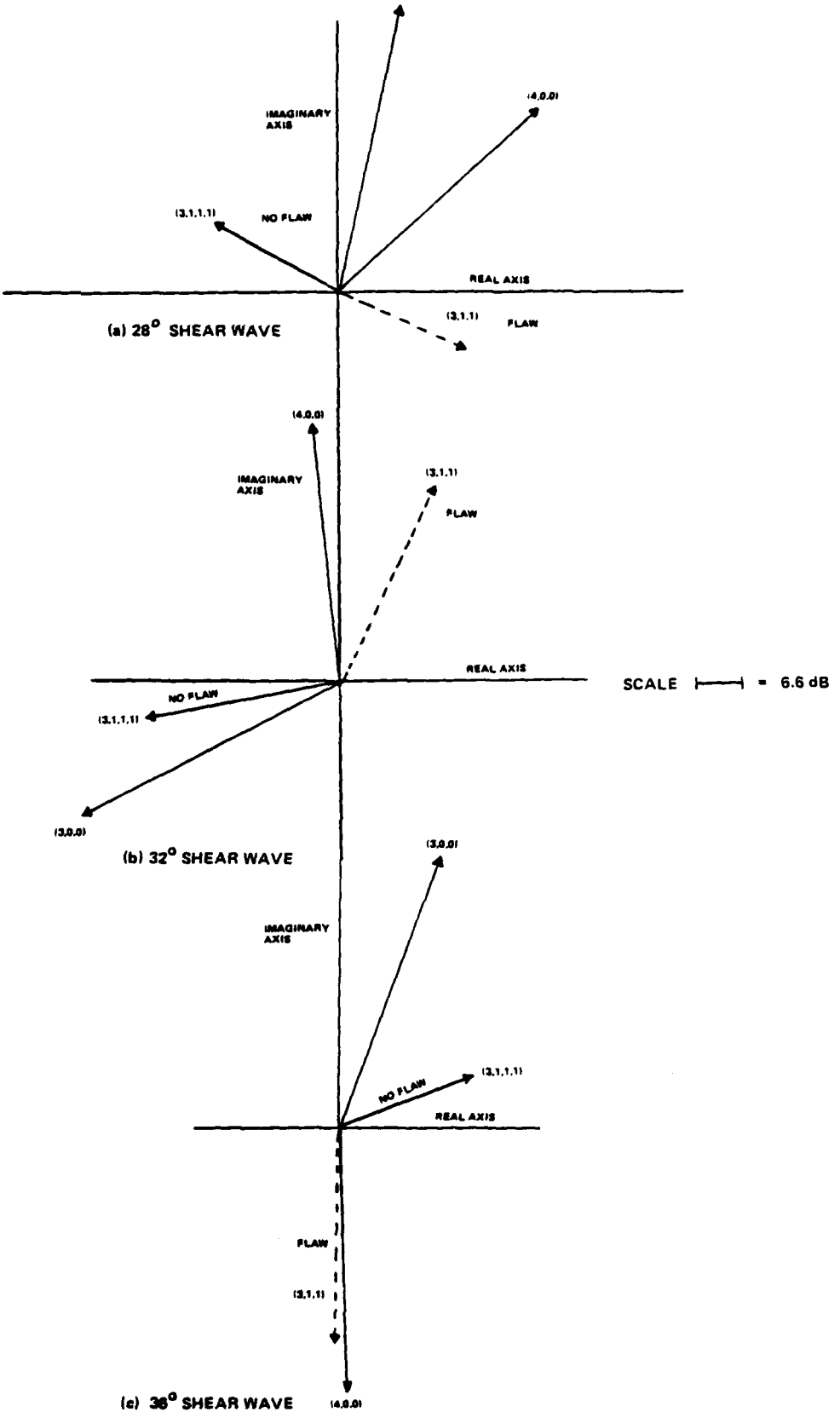

Figure 3.4. PHASOR RELATIONSHIPS AMONG THE RESPONSES FOR SELECTING OPTIMUM BEAM ANGLE

separation sets an upper limit on the period of the ultrasonic energy used to inspect and hence a lower limit on the frequency.

The time separation between the (3,0,0) and (3,,1,1) peaks is about 3 microseconds at this angle. Consequently a frequency higher than $(3\times10^{-6})^{-1}$ = 300KHz should be used.

Operating against this requirement for high frequency for resolution is that for low frequency for good transfer of energy through the rubber layer. The low Q of 10 found earlier for rubber (Reference 1) means that rubber attenuates ultrasonic energy at about 6 dB per millimeter per megahertz. Since the rubber path is 7.5 mm long round trip, each reduction in frequency of 1 MHz increases the signal by 45.0 dB. Consequently an operating frequency of 1 MHz was chosen as an acceptable compromise between amplitude and resolution.

EXPERIMENTAL RESULTS FOR BRONZE RUBBER STRUCTURES

4.1 APPARATUS

Data were collected in conventional pitch-catch fashion, using Harisonic 1 MHz, 1"x1/2" rectangular transducers. A Metrotek pulser was used to drive the pitcher and it also amplified the catcher signal. The amplified signal was displayed on a Tektronix Model 7854 digitizing oscilloscope.

The signal could be temporally averaged to reduce random noise, and typically averages of 10 waveforms were taken. The result was digitized and recorded on a magnetic cassette tape on a Hewlett Packard HP 9825 computer. Full header information was also recorded.

After collecting all waveforms the tape was copied onto 9 track tape so that it could be read at Tetra Tech.

Data were taken on a sample consisting of a bronze plate 6.35 mm in thickness bonded to a 3.175 mm thick rubber plate. The transducers were in contact with the bronze side of the structure, so this configuration simulated a disbond at the bottom of the first rubber layer of the actual 5 layer structure.

A good bond at the bottom of the first rubber layer was simulated by pressing a 6.35 mm thick bronze plate, well coated with ultrasonic couplant, against the side of the rubber layer. The lack of an epoxy layer here was not felt to cause an important difference in the returned signals.

Pitching and catching transducers were clamped in place so that their position and degree of coupling to the top bronze plate remained unchanged as the lower bronze plate was pressed in place and removed. Any variation in the observed waveform was therefore due to the presence or absence of the lower bronze plate.

A lesser separation of the pitcher and catcher is recommended by the results of the model study of Chapter 3. However, the shape of the shoes used here was such that they could not be brought this close together. The model predicts little loss in sensitivity from this case, however.

4.2 EXPERIMENTAL RESULTS

Waveforms with and without (Figure 4.1) the lower bronze plate show differences readily detectable by eye. To enhance these differences, the waveforms were subtracted, without scaling, resulting in the waveform of Figure 4.2.

This difference waveform shows two clear arrivals, which arrive at the expected time of the (5,1,1) and (6,1,1) responses. The conclusion drawn from Figure 4.3 is that the changes in the returned waveform due to a flaw at the bottom of the first rubber layer are clearly detectable, and that a system to detect this condition would be feasible. Figures 4.3 and 4.4 show the same set of waveforms observed at a different location to illustrate repeatability of results.

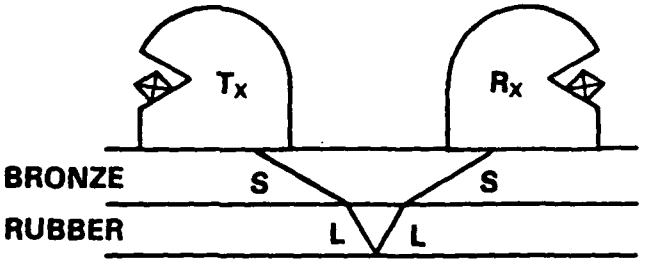

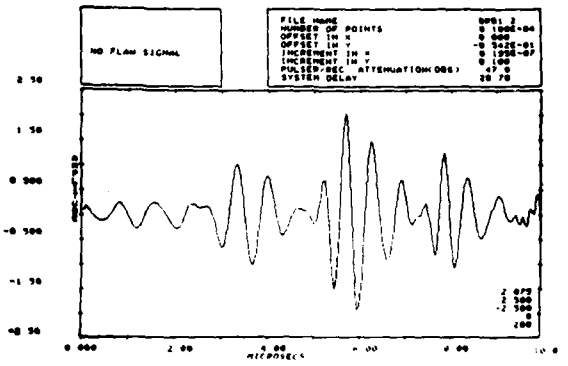

NO FLAW LOCATION 1

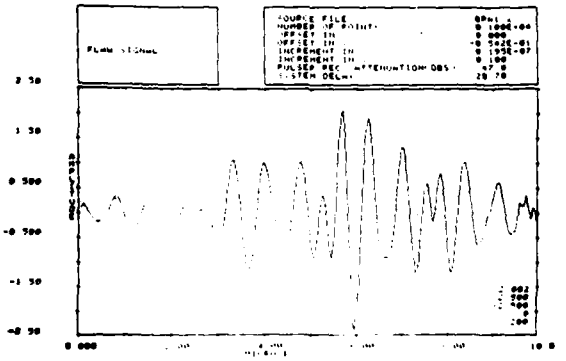

FLAW

T_X AND R_X FREQUENCIES: 1 MHZ
BEAM ANGLE IN BRONZE ≈ 32°
BEAM ANGLE IN RUBBER ≈ 28°.

Figure 4.1. INSPECTION OF TWO LAYERS FOR FLAW AT BOTTOM OF RUBBER

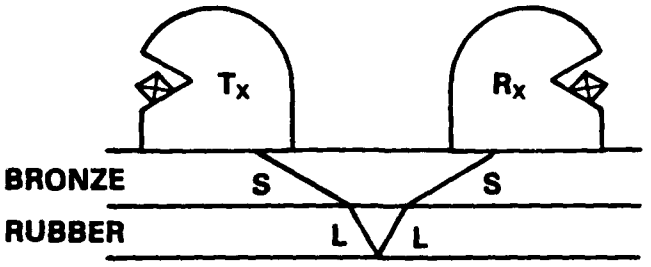

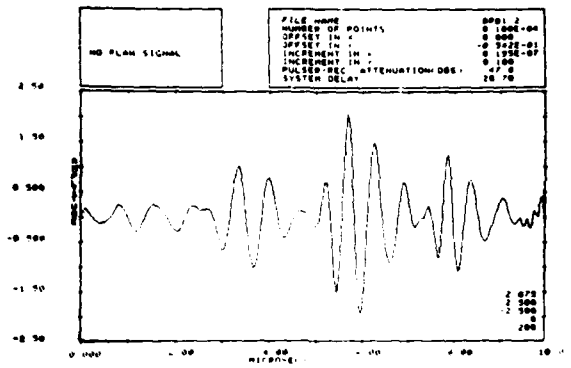

NO FLAW LOCATION 1

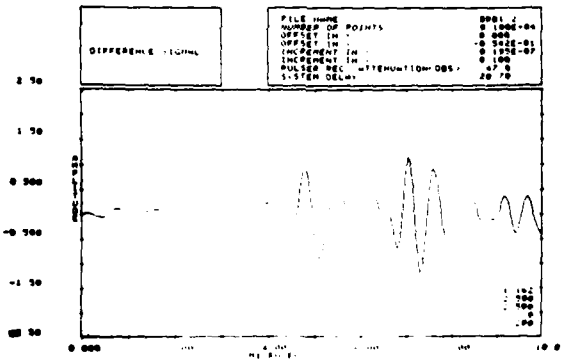

DIFFERENCE

T_X AND R_X FREQUENCIES: 1 MHZ
BEAM ANGLE IN BRONZE ≈ 32°
BEAM ANGLE IN RUBBER ≈ 28°

Figure 4.2. NO–FLAW AND DIFFERENCESIGNALS (FLAW RESPONSE *IN DIFFERENCE SIGNAL AT 5 AND 7 μs*

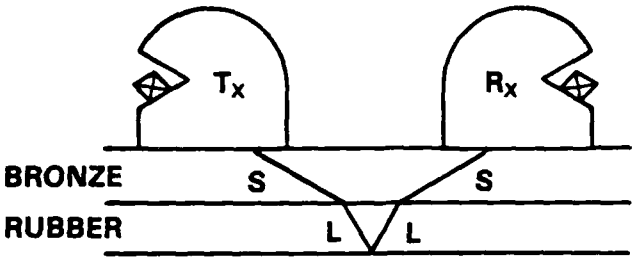

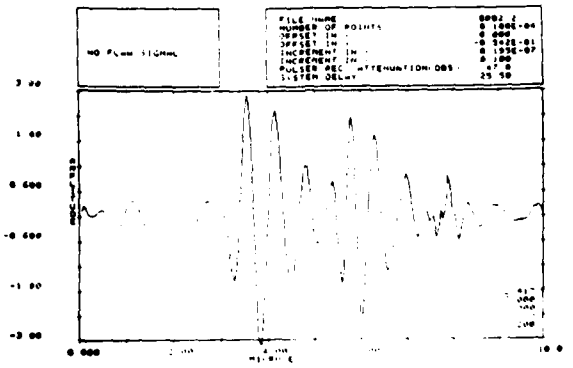

NO FLAW LOCATION 2

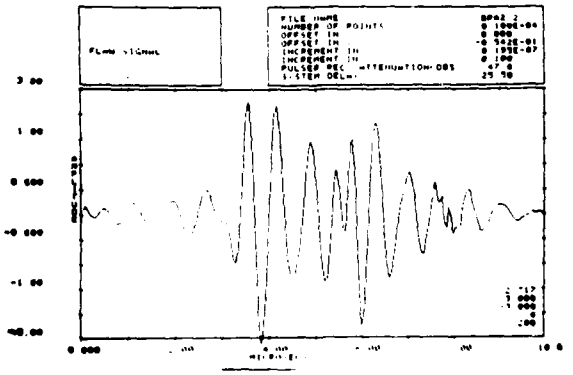

FLAW

T_X AND R_X FREQUENCIES: 1 MHZ
BEAM ANGLE IN BRONZE ≈ 32°
BEAM ANGLE IN RUBBER ≈ 28°

Figure 4.3. INSPECTION OF TWO LAYERS FOR FLAW AT BOTTOM OF RUBBER

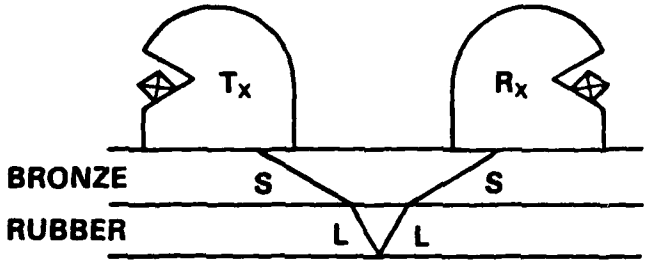

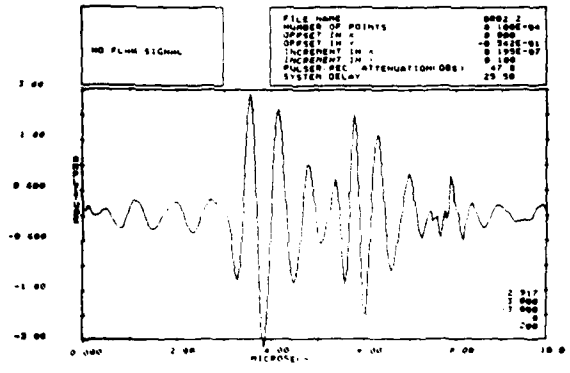

NO FLAW LOCATION 2

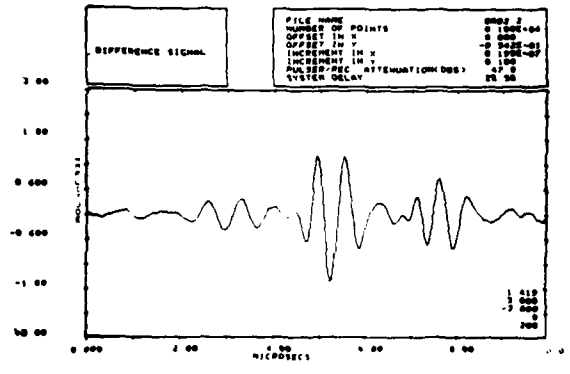

DIFFERENCE

T_X AND R_X FREQUENCIES: 1 MHZ
BEAM ANGLE IN BRONZE ≈ 32°
BEAM ANGLE IN RUBBER ≈ 28°

Figure 4.4. NO–FLAW AND DIFFERENCE SIGNALS (FLAW RESPONSE IN DIFFERENCE SIGNAL AT 5 AND 7 μs

Such a system would not use a subtraction technique like that used here, because differences in coupling and epoxy thickness at the bottom of the first bronze layer would preclude finding a "no-flaw" reference waveform suitable for all points. Other techniques, such as matched filtering, will probably be required, but the clear nature of the signals in Figures 4.2 and 4.4 suggest that they would have a very good chance of success.

CONCLUSIONS AND RECOMMENDATIONS FOR FURTHER WORK

Two main conclusions can be drawn from these results. First, the model developed here predicts experimental results with very good precision. Second, lack of epoxy at the bottom of the first rubber layer can be detected, using an experimental configuration chosen on the basis of the model prediction.

The model predictions include all quantities required to predict an observed waveform if the input waveform is known: arrival time and position, amplitude spectrum and phase spectrum. It can do so for both well bonded structures and for structures with lack of epoxy. Mode conversions are taken into account.

The utility of the model has been demonstrated by the successful detection of a disbond condition in a rubber-bronze structure, under operating conditions predicted to be optimum by the model. The results are such that we confidently expect that with further effort routine inspection for disbonds of this epoxy layer in the field could be undertaken.

It is recommended that work be continued in:

1. Signal processing to detect disbonds at the bottom of the first rubber layer under field conditions.

2. Construction of a prototype device to do so.

3. Investigation of techniques to inspect deeper layers.

4. Construction of samples to test these techniques.

5. Program to simulate other types of bonds - i.e., lack of adhesion... and incorporate into model.

REFERENCES

1. R. Shankar, S.S. Lane, and T.J. Paradiso, "Acoustic NDE of Multilayered Composite; Phase 1: Model Development and Inspection of Bronze Rubber Structures." Final Technical Report under Contract N-60921-81-C-0300 for the period September 1981 through June 1982. Prepared for NAVSEA 05R15

2. W.M. Ewing, W.S. Jardetsky, and F. Press. Elastic Waves in Layered Media. McGraw-Hill. 1957

END

DATE
FILMED

5 -83

DTIC